AD_____

AWARD NUMBER DAMD17-94-J-4133

TITLE: A Study of Ultrasonic Wavefront Distortion Compensation

PRINCIPAL INVESTIGATOR: Qing Zhu, Ph.D.

CONTRACTING ORGANIZATION: University of Pennsylvania
Philadelphia, Pennsylvania 19104-3246

REPORT DATE: August 1998

TYPE OF REPORT: Final

PREPARED FOR: U.S. Army Medical Research and Materiel Command
Fort Detrick, Maryland 21702-5012

REPORT DOCUMENTATION PAGE

Form Approved
OMB No. 0704-0188

1. AGENCY USE ONLY *(Leave blank)*	2. REPORT DATE	3. REPORT TYPE AND DATES COVERED
	August 1998	Final (1 Sep 94 - 31 Aug 98)

4. TITLE AND SUBTITLE
A Study of Ultrasonic Wavefront Distortion Compensation

5. FUNDING NUMBERS
DAMD17-94-J-4133

6. AUTHOR(S)
Qing Zhu, Ph.D.

7. PERFORMING ORGANIZATION NAME(S) AND ADDRESS(ES)
University of Pennsylvania
Philadelphia, Pennsylvania 19104-3246

8. PERFORMING ORGANIZATION REPORT NUMBER

9. SPONSORING / MONITORING AGENCY NAME(S) AND ADDRESS(ES)
U.S. Army Medical Research and Materiel Command
Fort Detrick, Maryland 21702-5012

10. SPONSORING / MONITORING AGENCY REPORT NUMBER

11. SUPPLEMENTARY NOTES

12a. DISTRIBUTION / AVAILABILITY STATEMENT
Approved for Public Release; Distribution Unlimited

12b. DISTRIBUTION CODE

The first objective of this research is to develop wavefront distortion compensation algorithms to improve spatial and contrast resolution of ultrasound imaging in the detection of breast lesions. The limiting factor for high resolution breast imaging is the acoustic wavefront distortion which is developed as coherent waves propagate inside the breast tissue. Wavefront distortion causes image degradation. We have developed a novel signal processing technique, called Toward Inverse Filtering (TIF), to compensate such distortion. *In vitro* one-way distortion compensation has shown that contrast resolution has been improved significantly with TIF. The second objective of this research is to develop a two-dimensional (2-D) ultrasound array for the implementation of the compensation algorithms in two-way propagation. We have constructed two prototypes of 2-D ultrasound arrays operating at 1 Mhz and 5 Mhz, respectively. In addition to the originally proposed work, we have developed a novel imaging method which combines ultrasound and near infrared diffusive light techniques. Experiments with phantoms using one-dimensional and two-dimensional combined arrays have shown that lesion acoustic and optical parameters can be jointly evaluated and the target detection sensitivity and specificity can be improved significantly. Since lesion acoustic and optical properties are different, the combined method has a great potential to improve breast cancer detection.

14. SUBJECT TERMS
Breast Cancer

15. NUMBER OF PAGES
39

16. PRICE CODE

17. SECURITY CLASSIFICATION OF REPORT	18. SECURITY CLASSIFICATION OF THIS PAGE	19. SECURITY CLASSIFICATION OF ABSTRACT	20. LIMITATION OF ABSTRACT
Unclassified	Unclassified	Unclassified	Unlimited

FOREWORD

Opinions, interpretations, conclusions and recommendations are those of the author and are not necessarily endorsed by the U.S. Army.

____ Where copyrighted material is quoted, permission has been obtained to use such material.

____ Where material from documents designated for limited distribution is quoted, permission has been obtained to use the material.

____ Citations of commercial organizations and trade names in this report do not constitute an official Department of Army endorsement or approval of the products or services of these organizations.

____ In conducting research using animals, the investigator(s) adhered to the "Guide for the Care and Use of Laboratory Animals," prepared by the Committee on Care and use of Laboratory Animals of the Institute of Laboratory Resources, national Research Council (NIH Publication No. 86-23, Revised 1985).

____ For the protection of human subjects, the investigator(s) adhered to policies of applicable Federal Law 45 CFR 46.

____ In conducting research utilizing recombinant DNA technology, the investigator(s) adhered to current guidelines promulgated by the National Institutes of Health.

____ In the conduct of research utilizing recombinant DNA, the investigator(s) adhered to the NIH Guidelines for Research Involving Recombinant DNA Molecules.

____ In the conduct of research involving hazardous organisms, the investigator(s) adhered to the CDC-NIH Guide for Biosafety in Microbiological and Biomedical Laboratories.

Q Zhu 9/14/98

PI - Signature Date

TABLE OF CONTENTS

5. INTRODUCTION 1

6. BODY 5

6.1. TIF wavefront compensation algorithm 5

6.2 Development of a two-dimensional ultrasound array and imaging system 11

6.3. Novel combined ultrasound and near infrared optical imaging 21

6.3.1. Combination of ultrasound with NIR cancellation technique 21

6.3.2. Combination of ultrasound with NIR tomography technique 27

7. CONCLUSIONS 29

8. REFERENCES 30

Publications 33

Presentations 34

Statement of work(original) 34

Revised statement of work 35

5. INTRODUCTION

Image degradation and phase deaberration

The major obstacle for achieving theoretical diffraction-limited ultrasound resolution in breast imaging is the acoustic wavefront distortion which is developed as coherent waves propagate through the inhomogeneous breast [A7-A12]. The primary distortion effect is the scattering of coherent energy. As a result, the target strength is reduced, the image lobe is broadened [A7-A8], the background level is increased and therefore the image contrast is reduced [A2,A11]. The secondary distortion effect is the multipath interference which produces ghost image artifacts or false targets in addition to true targets in the image [A9]. Adaptive compensation of wavefront distortion is an active area of current research [A13]. Two basic *phase* deaberration algorithms have been developed in [A15-A17]. These algorithms adjust time delays of received waveforms at different elements of a phased array to compensate delay errors due to an inhomogeneous medium and consequently reduce the scattered energy. These phase deaberration algorithms are very useful to partially remove phase distortion and build up the strength of the coherent field. Many extensions of the basic phase deaberration algorithms have been developed to improve the performance of phase deaberration algorithms.

These phase deaberration algorithms have shown improvements in image quality in phantom, in vitro and in vivo pilot studies; however, the improvements are moderate because of difficulties of accurately estimating arrival time errors and because of wavefront amplitude distortion. Residual phase errors and amplitude distortion increase sidelobe level in the image. Measurements of 16 breast specimens obtained from a large 2-D array have shown that the contrast of point-source images is about 10 dB lower than that obtained from a homogeneous water path even when the phase errors are completely compensated [A3]. Measurements of 44 in vivo breasts obtained from a 1-D large array have shown that the average sidelobe level in point-source images caused by the amplitude distortion is 17 dB higher than that obtained from a homogeneous medium [A11]. Therefore amplitude distortion can cause a serious loss of contrast. The method we developed during the first two years of this project, called TIF (defined later), compensates for amplitude distortion [A2-A4].

Figure 1 shows simple models to illustrate the effects of wavefront distortion upon a point source image or its angular spectrum (intensity distribution), and the effects of phase deaberration. Without medium induced distortion, we should see the diffraction limited coherent spectrum shown in Figure1a. In the presence of medium induced scattering, the overall angular spectrum is the sum of coherent and scattered spectra [A18] as shown in Figure1b. Because of scattering, the coherent spectrum is broadened and reduced in strength. The background level is increased and, therefore, image contrast is reduced. As shown in Figure1c, the implementation of a phase deaberration algorithm results in the partial removal of phase distortion and therefore strengthens the coherent spectrum; yet a significantly high incoherent background level remains in the spectrum due to residual phase errors and uncompensated wavefront amplitude distortion. Any phase-deaberration procedure that provides a better phase error estimate than that of basic algorithms would reduce this background level [A3]. Wavefront-deaberration algorithms that compensate wavefront amplitude distortion can further reduce this background level [A3]. In the case of multipath interference (Figure1d), the scattered energy removed by the phase deaberration process strengthens the primary spectrum (sharp peak) by folding the removed scattered energy into the primary field. As a result the ratio of the primary lobe to interference lobes is improved (Figure1e).

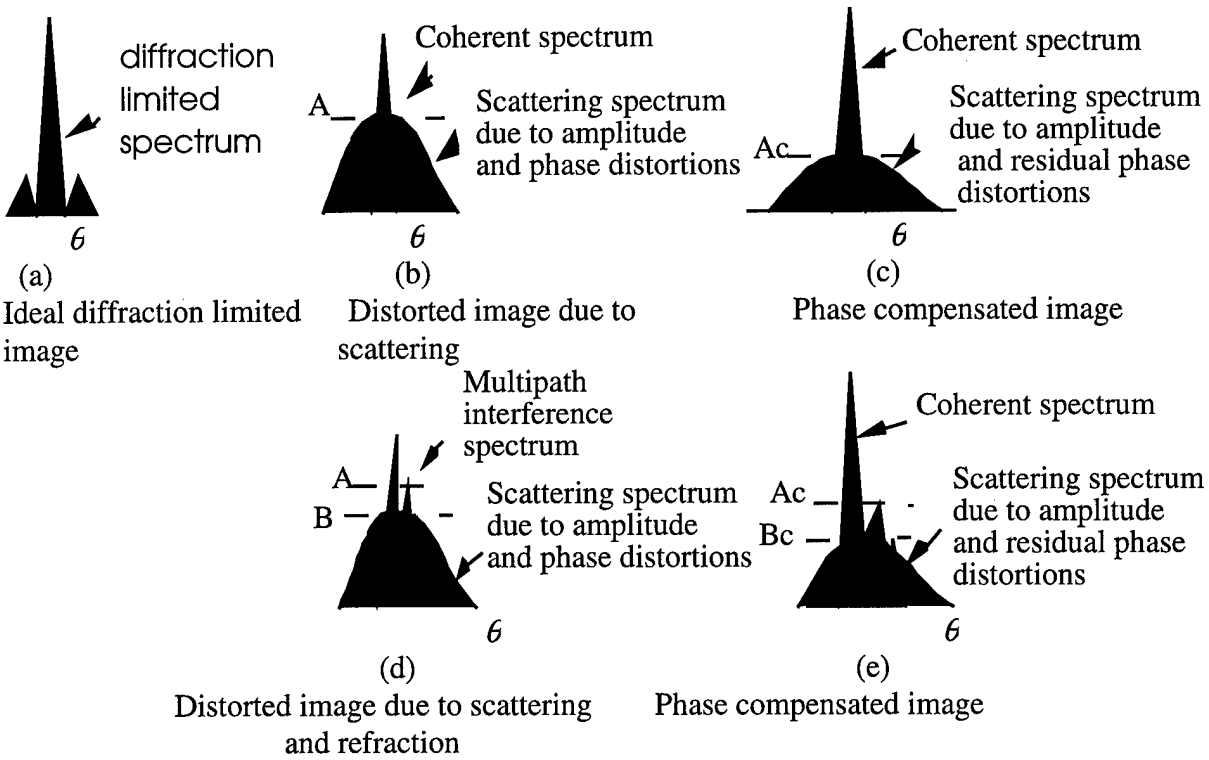

Figure 1. Statistical models of angular source intensity distribution. (a) diffraction limited spectrum. (b) Scattering induced distortion. The spectrum is the sum of coherent spectrum and scattering spectrum. (c) After partial phase compensation of scattering spectrum of (b). Contrast resolution is improved. (d) Multipath interference induced distortion. (e) After phase compensation of (d).

Compensation of ultrasonic wavefront distortion

Full compensation of wavefront distortion presents a more difficult problem because there is no general way to reduce wavefront amplitude distortion. The iterative time reversal focusing (TRM) technique has been introduced in [A24]. The transmission beam quality has been improved using TRM compared with the beam quality using time-delay focusing techniques when a thin aberrating layer is placed between a point target and a receiving array and is located closer to the target. However, TRM has limited applications in medical imaging because it requires the existence of strong point scatterers which are rarely found in the body. In addition, TRM is a matched filtering approach which optimizes signal-to-noise ratio for detection purposes but not image contrast which is a critical parameter for medical imaging. TRM produces high sidelobes in transmitting beams [A25]. Liu and Waag [A26] have improved time-delay compensation by backpropagating the received waveforms to an optimal distance and then performing time-delay compensation (BPT) at this distance. Backpropagation partially compensates amplitude distortion produced by wave propagation from the backpropagation distance to the receiving aperture. BPT could be a useful tool to correction distortion produced by the abdominal wall. Since the abdominal fat layer is the major source of distortion, the layer thickness is an appropriate backpropagation distance. The parallel adaptive receiving beam technique, called PARCA, has been proposed in [A27-A28] which estimates and removes the sidelobe artifacts due to interference between targets. PARCA when used in combination with phase deaberration techniques has shown promising results to clean up sidelobes inside vessels in abdominal images [A29].

We have developed a more general approach in frequency domain, called Toward Inverse Filtering (TIF), to compensate for frequency dependent wavefront amplitude distortion in addition to phase deaberration [A2-A4]. The well known Inverse Filtering (IF) technique [A1] is optimal from the standpoint of imaging fidelity but lacks stability. TIF approaches the performance of IF by compressing the frequency components of the received element signals. Since the TIF compression replaces the IF inversion, TIF is stable. One-way (receive only) experiments with breast specimens have shown that TIF represents a substantial improvement in contrast resolution over other deaberration algorithms, offering the potential for better visualization of low contrast lesions. The results were reported in [A2-A4] and are summarized in Section **6.1A** .

High resolution, high contrast breast imaging implies seeing a black cyst or a hypoechogenic lesion 60 dB weaker than a brightly speckled target. This implies that 30 dB contrast has to be achieved in one-way transmission and reception. In the first two years of this project, we found that by applying time-delay correction to *in vitro* one-way breast data, time-delay correction successfully suppressed scattered energy and folded it into the target image, restoring the mainlobe diffraction shape to the -20 dB region [A3,A33]. The one-way data were received from a 2-D aperture. We also found that an additional 4-5 dB improvement can be obtained by applying Liu and Waag's back propagation algorithm [A26]. Additionally, with TIF, we are able to improve all the correction algorithms and restore the mainlobe diffraction shape down to -30 dB [A3] which is the necessary one-way condition to image small breast lesions and lesion architecture. If comparable distortion compensation can be accomplished on transmission, contrast resolution in the neighborhood of bright reflectors could reach 60 dB. This would be an invaluable assist in clinical ultrasound. However, no two-way (transmit-receive) RF data set is available with a full size 2-D array. We do have access to two-way data sets from http://bul.eecs.umich.edu using a phantom and a 1-D array. With it, we can see promising evidence of the value of TIF in two-way imaging. Most of the evidence is qualitative clinical evaluations. Some quantitative measurements have been made. The experimental results are summarized in Section **6.1 B** in this report.

2-D *Compensation of wavefront distortion needed in two-way propagation*

The complex compensation vector for each channel is derived from the RF data received across the array. Neighboring data are most valuable. However, it is insufficient to obtain these data from a 1-D array because the aberrated field is not confined to any single plane. Also, when nearby data are noisy or are otherwise corrupted data smoothing from additional 1-D rows in the transducer is helpful. Hence the receiving field should be sampled in two dimensions and therefore an array that samples the field in two dimensions is required to acquire the optimum data set for setting the complex deaberration weights in the aperture. Under general imaging condition, the 2-D array should function both as transmitting array and receiving array.

However, 2-D arrays that operate in two-way propagation are currently in research stages and are not commercially available. In our original proposal (third year SOW,1996-1997) we proposed to design a two-dimensional (2-D) concave ultrasound transducer which would reduce breast-curvature caused refractive-distortion effects upon images in addition to being a tool for implementing 2-D compensation algorithms. We did not propose fabrication of such arrays. To accelerate the transfer of our technique to clinical breast imaging studies, we decided to fabricate our own 2-D arrays. But concave shape

introduces complications in fabrication. Since breast-curvature caused distortion effects can be largely reduced by using a 2-D planar array compressing against the examined breast, we have focused our research on design and fabrication of 2-D planar arrays. The results of array and imaging system constructions are reported in Section 6.2. The modified SOW submitted to Deputy Director for Science Management, Dr. Patricia Modraw, on April 1998 reported this change.

Novel combined ultrasound and near infrared diffused light imaging

In addition to the work originally proposed in this application, we have done additional work on combining ultrasound and near infrared (NIR) diffusive light techniques for breast imaging. The objective is to use complementary features of ultrasound and NIR to increase detection sensitivity and specificity of breast lesions. Experimental results with phantoms were very encouraging, and clearly indicated that this novel method could be potentially very important. Although this work was not proposed in the original proposal, it was an important discovery and was directly related to PI's breast cancer research. Since this award is in the career development category, the PI will reported this work in Section 6.3. The rationale of developing the combined method is given as follows.

Ultrasound is frequently used in conjunction with mammography to differentiate simple cysts from solid lesions. When all criteria for a simple cyst are strictly adhered to, the accuracy of ultrasound is 96%-100% [C1]. Literature data on early detection of small solid lesions are sparse. An early paper by Dam et al. reported the ultrasound sensitivity in the detection of palpable solid masses less than 2 cm in size was 71% which was about 10% less than the sensitivity of physical examination [C2]. A recent paper by Paramagul et al. reported the sensitivity in the detection of small invasive lobular carcinomas (<1 cm) was only 25% [C3]. Early reports indicated that ultrasound specificity was low due to the considerable overlap of benign and malignant lesion characteristics [C4-C5]. More recently, the imaging capability of ultrasound equipment has markedly improved. Studies reported by Stavros et al. [C7] were very encouraging. In [C7], a total of 750 *palpable* solid breast lesions were studied. Fifty percent of these lesions were between 0.5 and 1 cm in size with less than 5% of these lesions being smaller than 0.5 cm. Despite the known overlap features in some lesions, ultrasound was able to correctly classify 123 of 125 malignant lesions as intermediate or malignant. It is expected that additional NIR optical properties will provide more diagnostic information to further classify the intermediate group, thereby improving ultrasound specificity.

Over the last two decades, the scope and importance of research being conducted on optical methods for spectroscopy and imaging has increased dramatically [C8-C9]. Optical spectroscopy and imaging of body structure and function is made possible by a spectral window within tissues in the near infrared range (700 - 900 nm), wherein photon transport is dominated by scattering rather than absorption. To a very good approximation, these NIR photons diffuse through relatively thick tissues, such as 10-15 cm of a large human breast. The diffusion approximation enables quantitative separation of tissue absorption from tissue scattering.

NIR light in general has high sensitivity and specificity because tumors differ from normal tissue as follows: 1) The amount of blood needed to serve the tumor's metabolic needs is increased over that of normal background tissue; 2) Hemoglobin desaturation in tumors is increased due to the high oxygen demand of cancers; 3) Light scattering properties of the tumor are expected to be enhanced due to the increased mitochondria population with respect to the background of normal cells [C10], 4) The

angiogenesis phenomenon [C11] allows tumor identification by observing the delivery of contrast agents, such as the well-characterized NIR absorber indocyanine green (ICG), through the permeable vascular beds to the extravascular space surrounding the tumor. The intense absorption band of ICG at 800 nm affords a high contrast of the tumor extravascular space as compared with the background capillary network of the normal tissue. In addition, ICG has an interesting redshifted fluorescence property [C12]. That is, it absorbs radiation at the source wavelength of 780 nm and reradiates photons at 830 nm. In this process, the tumor extravascular space is converted into an increased source of secondary diffuse waves with reduced background. Finally, NIR contrast agents could potentially be linked to tumor-specific antibodies or to specific sites in the tumor such as their mitochondria membranes.

The promise of the optical method led to the first clinical studies of the diffusive wave optical technique in the human breast. In those experiments [C13-C14], diffuse waves were applied to the human breast in the transmission mode in a conventional X-ray "firm-compression", parallel-plate, source-detector geometry. The investigators used the frequency-domain method, i.e., the intensity of light is modulated at a RF frequency, and diffusive wave amplitude and phase data are obtained and then processed using a phase-corrected, linear, back-projection procedure [C14]. The method gave images of tumors in 73% of cases [C13] congruent with X-ray mammography of the same breast. In a second set of studies by a different group [C34], clear differences in tumor optical properties were found including a surprisingly large variation in water content. These initial results are very encouraging, and clearly indicate that the technique is potentially important.

However, there are intrinsic difficulties in obtaining images with high spatial resolution because of the diffuse nature of light propagation in human tissue. Most imaging algorithms are based on computer tomographic (CT) reconstruction techniques [C15-C22]. Tomographic approaches require one to invert the diffusion equation or to use time-intensive iterative techniques. The problem is more complicated than the x-ray CT approach because photons do not travel along straight lines. Currently, typical reconstructions can distinguish simple structures of approximately 1 cm in size; sharp edges are typically blurred by a few millimeters [C8].

Clearly the optical method offers interesting new routes to better tumor specificity. Unfortunately, the relatively poor resolution of the optical reconstructions makes it difficult to take full advantage of this contrast. Co-registered ultrasound images could provide a new way to utilize optical contrast and ultrasound imaging capability and to independently distinguish tumors from normal breast tissues.

6. BODY:

6.1. TIF wavefornt compensation algorithm

Typical example of one-way TIF correction with 2-D Array

TIF theory was published in [A2]. This section gives a typical experimental example and summarizes the results. In the breast, refraction and scattering are significant sources of distortion [A3,A9]. Refraction occurs at interfaces between fat and glandular tissue which causes multiple arrivals at the receiver, resulting in image artifacts that can look like and be mistaken for targets. Scattering raises the background level above the sidelobe level of the transducer and thereby reduces contrast resolution. Figure 2 shows both phenomena in a diffraction pattern or a point source image obtained from one breast specimen [A3]. Data from other samples are given at the end of this section. Figure 2a shows highly asymmetric interference pattern typical of refraction-induced multipath. Outer contour is -10 dB level. Peak of false target to left of main lobe located in

the middle is -6 dB. Figure 2b shows the more symmetrical pattern typical of scattering which generally appears at a lower contour level. False target-to-scattering ratio is 16 - 6 = 10 dB in this case.

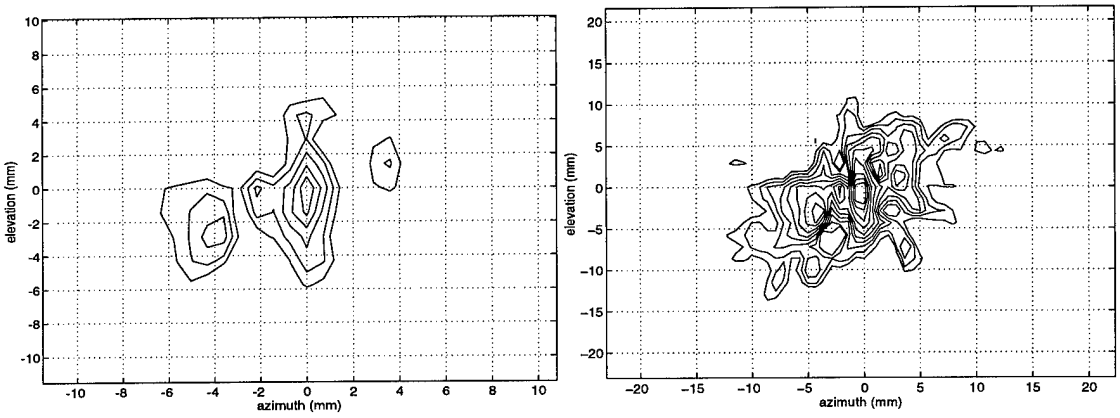

(a) -10 dB (breast 006) (b) -16 dB (breast 006)

Figure 2. 2-D contour maps of point source image measured one-way in water tank through 4-cm thick breast specimen (brs006). Contour spacing is 2 dB. (a) shows highly asymmetric interference pattern typical of refraction-induced multipath. Outer contour is -10 dB level. Peak of false target to left of main lobe is at -6 dB. (b) at -16 dB outer contour level the more symmetrical pattern typical of scattering appears. Note the change of scale from (a) to (b).

The data were taken in a 2-D, *in vitro* , water bath measurement system using a 4-cm breast specimen surgically removed from a medically obese woman. Propagation was one way [A3,A12]. The breast specimen was placed between a hemispherical source and a 92-mm, 1-D linear receiving array (see the following diagram for illustration). The array was translated 46 mm perpendicular to its axis to form a synthetic 2-D array 92 mm x 46 mm. Element pitch in the receiving transducer was 0.72 mm and a reflecting mask reduced the receiving elevation to 1.44 mm. The frequency was 3.7 MHz and the bandwidth was 2 MHz. Waveforms were measured at each element, from which 2-D wavefronts were reconstructed as functions of time. 2-D spatial image data (point source image) were obtained by detecting the peak pressure value at each position in the image plane within the transient period. Contour plots were obtained at different levels.

The quality of the measurement system is acceptable at least to the level of -30 dB. This is demonstrated by the measurements in Figure 3 taken in the water tank without the tissue sample, which show that the system diffraction pattern, at outer contour levels of -10 and -30 dB, has a single clean lobe.

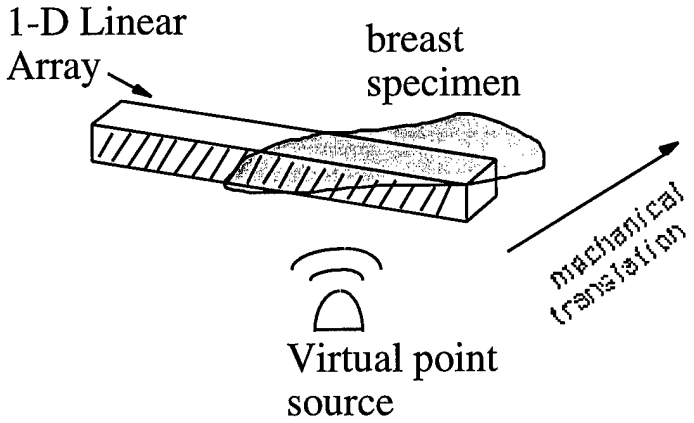

Illustration of 2-D in vitro measurement system.

Figure 4 illustrates image quality improvement given by the proposed TIF wavefront deaberration procedure [A3]. Two variants are shown. Contour spacings are 3 dB. Outer contours are at -30 dB. Both eliminate the false targets (refraction, see Figure 2a) and the raised background level (scattering, see Figure 2b) down to at least -30 dB. The patterns are very close to the system diffraction pattern (Figure 3b). Square rooter TIF with backpropagation (BP) and phase compensation (PC) (defined below), and 4th order rooter TIF and PC, as shown in (a) and (b), restore the diffraction-limited image to a -30 dB level. The improvements are enormous .

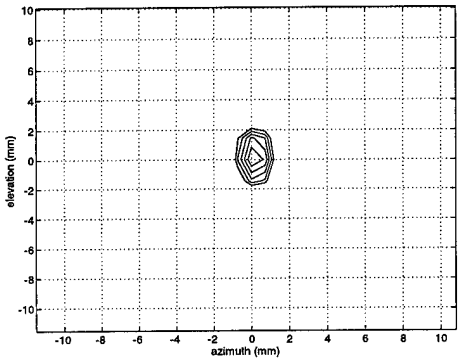

(a) -10 dB level (water path).

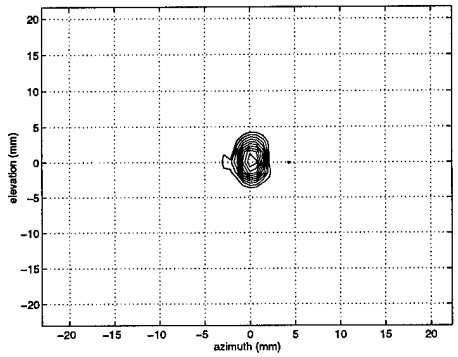

(b) -30 dB (water path).

Figure 3. Measured one-way diffraction patterns of system at -10 and -30 dB demonstrating that main lobe remains down to - 30 dB. Water path only. Contour spacings are 2 and 3 dB, respectively. Note the change of scale from (a) to (b).

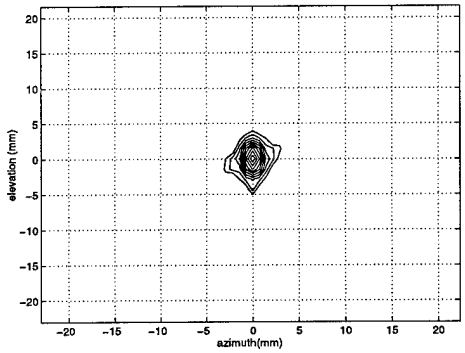

(a) TIF (at -30 dB): Square rooter with BP and PC (breast 006)

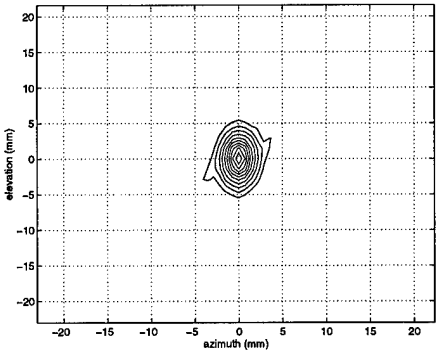

(b) TIF (at -30dB): Fourth rooter with PC (breast 006)

Figure 4. Images of same point source after wavefront deaberration by TIF. Outer contours are -30 dB.

A comparison is made in Figure 5 with other major wavefront compensation methods described in the literature. (5a) is time delay compensation (TDC) of the echo waveform, which is the most commonly employed [A15] and (5b) is phase compensation (PC) [A17], which is approximately TDC at each frequency component in the signal spectrum. Both are shown at the level of -30 dB. (5b) is somewhat superior. Both reduce but do not remove the false target lobes. Both show the order of 15 dB suppression of the background scatter level. Neither approaches the system diffraction pattern. (5c) shows the performance of the dominant scatterer algorithm (DSA) [A30], which is a wideband matched filtering method [A2]. The outer level is -16 dB, where it may be compared to the uncompensated image (2b) at the same level. The improvement in suppressing scattering is evident but the false targets are actually accentuated. Thus the net improvement is small compared to the other methods, as seen in Figure 4 with TIF or in (5d) with TDC at -16 dB.

These and other experiments with breast tissue, in one-way propagation tests with a 2-D array [A3], show TIF to be the best, BPT next, PC and TDC behind and wideband DSA a distant fourth.

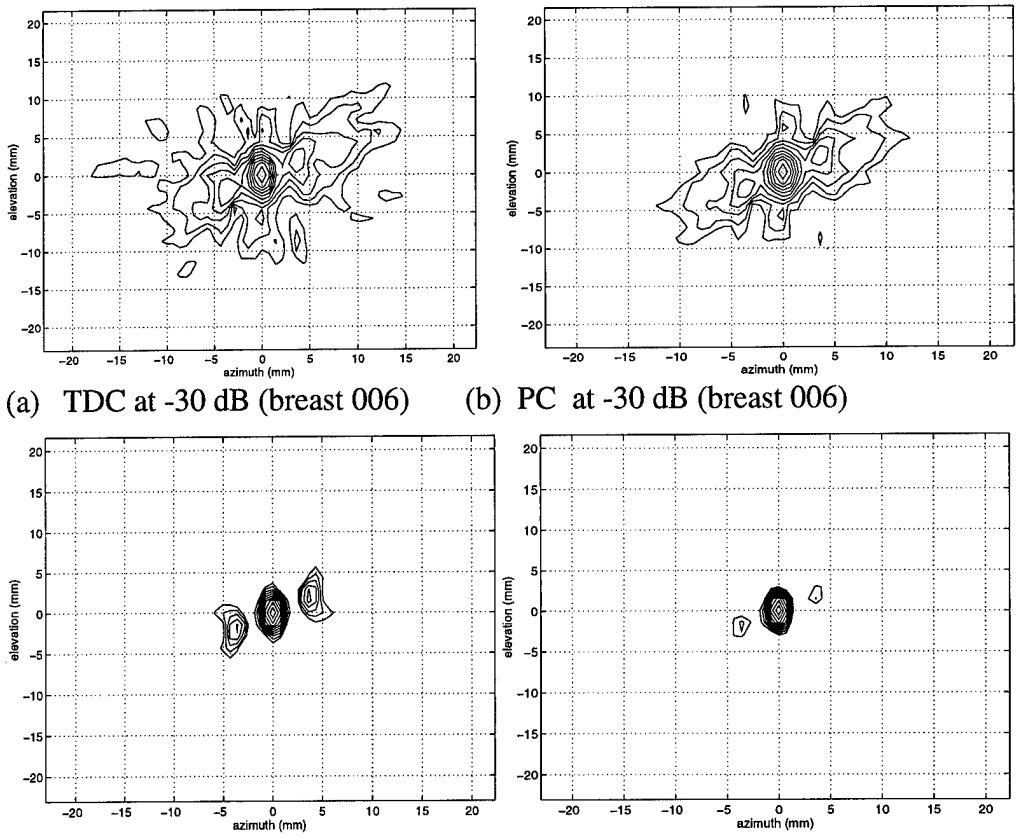

(a) TDC at -30 dB (breast 006) (b) PC at -30 dB (breast 006)

(c) Wideband DSA at -16 dB (breast 006) (d) TDC at -16 dB(breast 006)

Figure 5. Other deaberration methods.

Two measures were used to evaluate the correction: mainlobe diffraction pattern and energy ratio (energy outside the mainlobe/energy inside the mainlobe). The statistics obtained from 16 breast specimens are given in [A3]. In summary, time-delay compensations, which leave the magnitude of the wavefront unchanged, have recovered the average mainlobe diffraction shape down to -19.4 dB (std. 2.73 dB) compared with the average -4.0 dB (std. 1.6 dB) without phase deaberration. The backpropagation method is shown to recover the average mainlobe diffraction shape down to -24.0 dB (std. 1.7 dB). The use of TIF improves the performance of the compensation techniques significantly, and the mainlobe diffraction shape can be recovered down to the average of -30.3 dB (std. 2.2 dB). The energy ratios are 214% (std. 130.1%), 25.1% (6.9%), 12.8% (std. 2.9%) and 2.9% (std. 0.6%) with no compensation, time-delay compensation, BPT and TIF, respectively.

Example of Two-way TIF Correction with 1-D Array

Figure 4 showed that the badly distorted radiation pattern seen in Figure 2 was deaberrated down to -30 dB with TIF when a 2-D receiving aperture was used. Propagation was one-way. If comparable distortion compensation can be accomplished on the echo path, contrast resolution in the neighborhood of bright reflectors could reach 60 dB. This would be an invaluable assist in clinical ultrasound. To test this supposition two-way propagation TIF experiments are needed.

Since commercial scanners operate with 1-D arrays, we have conducted initial experiments [A31] which show that TIF is promising. The experiment was designed to test the feasibility of TIF in pulse-echo imaging. The

test target was the low contrast cyst at coordinates (250,425) in Figure 6a. Seen below the cyst is a region with an altered texture and poorer angular resolution, a result of interference between ultrasound energy diffracting around the cyst and energy, with different speed, passing through it. The textural difference provides a clinical clue, when the contrast is low, to the presence of a lesion that is insufficiently differentiated from the surrounding tissue to be easily observable. Figure 6b (a section that contains the cyst) shows the effect of an aberrating plate, made of RTV silicone rubber, placed between the transducer array and the phantom. The plate produces phase distortions within 2π and amplitude distortion. The cyst is lost (arrow) and the contrast is too poor in the interference region below it to provide much of a clue to the existence of the lesion. Furthermore, scattering induced by the phase plate raised the background level to destroy image dynamic range almost everywhere. Figure 6c shows the result of phase-only correction. The image dynamic range is restored to some extent but the contrast is still too poor in the cyst region to ensure definite detection.

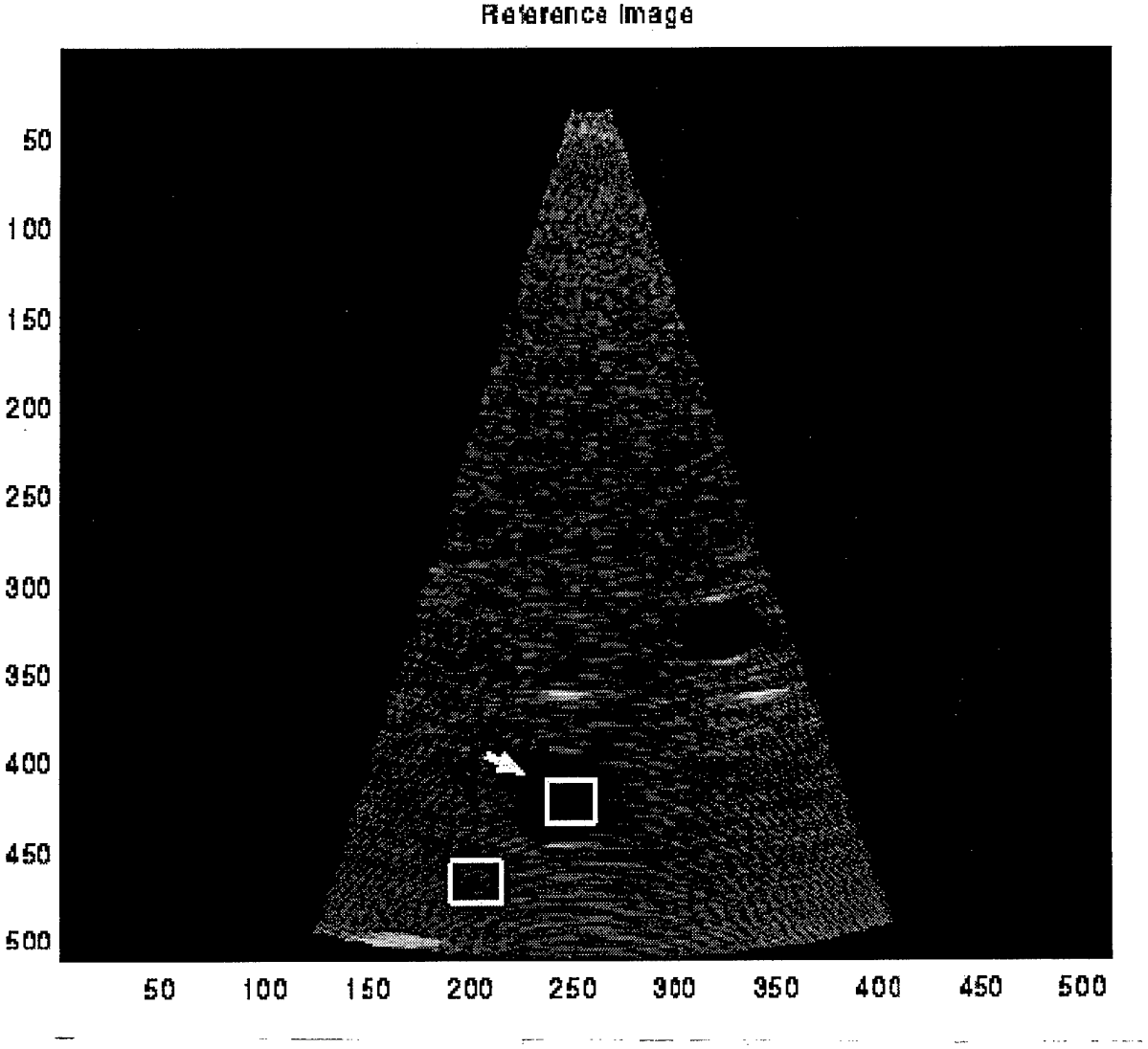

Figure 6. (a) Phantom image without aberration

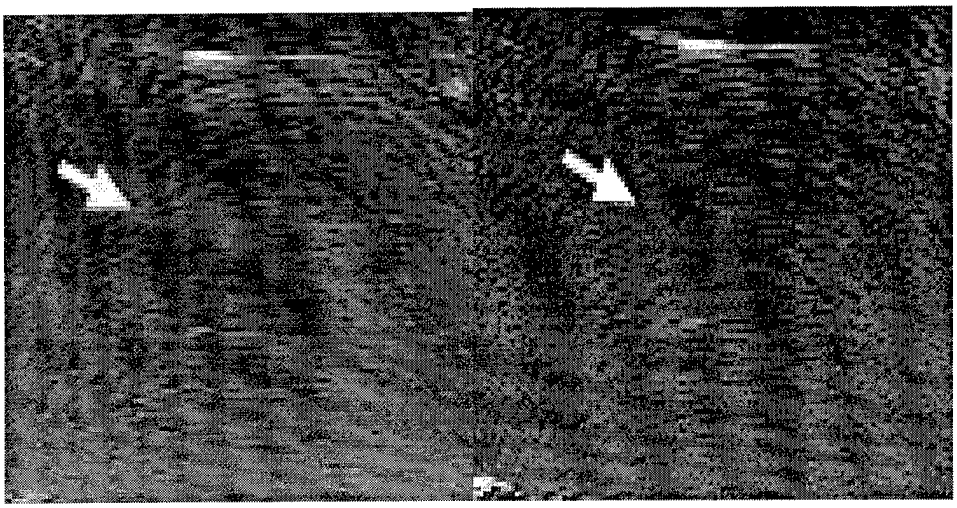

(b) With aberration, no correction (c) Phase-only correction.

(d) Deaberration by TIF

Figure 6. (a) B-scan phantom image with lower left cyst at coordinates (250,425). (b) The portion of the image containing the lower left cyst when the aberratting layer was placed between the phantom and the array. Lesion lost in scatter induced by aberrator. (c) Phase-only correction. The image dynamic range is resorted to some extent. (d) TIF image. General image contrast is restored, lesion contrast plus the specular reflections from posterior wall and, to lessor degree, from the anterior wall of the lesion allows lesion to be detected. Altered texture below cyst can be seen, increasing confidence in a successful reading. All images displayed with logarithmic scale over 35 dB.

Figure 6d shows TIF reconstruction. General image contrast is restored, lesion contrast plus the telltale specular reflection from the posterior wall of the lesion, and to a lessor degree from the anterior wall, allows the lesion to be detected, and the altered texture below it can be seen, increasing confidence in a successful reading. All images were displayed on a logarithmic scale over a 35 dB dynamic range.

The above qualitative evaluations were performed by Dr. Emily Conant, Chief of the Breast Imaging Section of the Radiology Department of the University of Pennsylvania. The comparison between phase-only correction and TIF was blind.

A quantitative measure of improvement can be obtained with the contrast ratio (CR). CR is defined as the difference in dB between the mean brightness within a low contrast region such as a cyst and the mean brightness in a neighboring region. For the low contrast cyst image of Figure 6a, data within the superimposed boxes were used to compute the means. The reference image was taken with no aberrating layer. Its CR is 3.3 dB. The uncorrected image, after insertion of the aberrating layer, is shown in Figure 8b. Its CR is 2.6 dB. Phase-only correction (Figure 6c) raised CR to 2.9 dB and TIF (Figure 6d) further increased CR to 3.3 dB, thereby completely restoring the contrast.

Obtaining RF channel data for work of the kind is very difficult. The data for this two-way pulse-echo phantom experiment were downloaded from the world-wide web at http://bul.eecs.umich.edu (detailed description of the data is in [A32]). All data sets were acquired with a 1-D, 64-element, 15.4-mm array operating at 3.33 MHz with a fractional bandwidth of about 35%. Each complete data set consisted of 4096 (64x64) RF A-lines with each line sampled at a rate of 17.66 MHz with 10 bit analog-to-digital conversion. Each line represents a single element acting as a transmitter and another, independent element acting as a receiver. Three data sets were obtained from a standard graphite-gel AIUM resolution phantom and two were used in our preliminary experiments. The sampling rate of each RF A-line was increased by 8 times using bandpass interpolation. Therefore, wavefront compensation and beamforming are performed with 142 MHz sampling rate, corresponding to a phase accuracy of better than $2\pi/43$. One RF pattern at each scan angle was synthesized from each data set. B-scan images without correction were formed by adding RF signals across the array at each scan angle. The unit-lag phase deaberration algorithm [A15] with a simple modification was used to correct delay errors of RF signals produced by the aberrating layer. TIF square root amplitude compression was implemented after phase correction. Fast Fourier Transforms of waveforms at each element of the aperture were taken within a window centered on the low contrast lesion (lower left in part a). Images were formed with fixed focusing on transmission and reception at 90 mm range (center of the lower cyst), and were displayed on a logarithmic scale over a 35 dB dynamic range.

6.2. Development of a two-dimensional ultrasound array and imaging system

We have developed two prototypes of two-dimensional ultrasound arrays. One array of 2.5 cm x 2.5 cm size operating at 1 Mhz frequency was built first. This frequency is not high enough for medical applications. However, the array fribrcation is relatively simple compared with high frequency arrays because the array element is larger at lower frequencies. The objective is to gain expertise for building high frequency arrays. The array is made of piezoelectric composite consisting of PZT (lead zirconate titanate) ceramic rods in a polymer matrix. The transducer head contains the transducer layer with ground metalization on the front side and individual electrodes on the back side. Connections to the back electrodes of all operational piezo-elements are provided through wires soldered to a PC board. Design, fabrication and preliminary testing of the fabricated array are summarized in Section 6.2.1. Another simple 2-D array operating at 5Mhz was also built. This array is made of 20 small (1.5 mm in diameter) PZT commercial crystals which are distributed in a 2-D rectangular matrix. The resolution of the second array is not high because of the sparse quality of the array. However, this array serves our immediate need to test deaberration algorithms and to study co-registration of ultrasound and NIR optical images (Section 6.3). The front end electronic system which supports the data acquisition of the 2-D crystal array is also built. This system is used to replace the proposed modified electronic system of an old ultrasound commercial scanner (second year SOW). In addition, this digital system is better than the proposed modified analog system. The construction of the array and the data acquisition system is summarized in Section 6.2.2.

6.2.1. 1MHz prototype array

A. Transducer Materials and Interconnects

A 1-3 type of piezoelectric composite consisting of PZT (lead zirconate titanate) ceramic rods in a polymer matrix serves as the material from which two dimensional addressable transducer arrays are constructed [B1]. Composites (combinations of two distinct solid phases with different connectivity patterns) can greatly enhance material utilization and properties by the synergy generated, the properties of the combination being better than the individual properties. Composites provide a much wider range of material properties than those of the standard ceramic and polymer transducers and are being actively studied in the medical ultrasonic field [B2].

In our design the individual rods with end faces individually electroded serve as transducer elements. Ideal characteristics are strong electromechanical coupling for efficient energy conversion, low acoustic impedance for good transmission into tissue, and a reasonably large dielectric constant for efficient electrical impedance matching [B3]. Further advantages of strictly periodic composite materials are control of lateral transducer resonances and reduction of crosstalk between individual electrodes in transducer arrays.

By utilizing the optimized 1-3 composite transducer design, high transmit efficiency, high receive sensitivity and broad bandwidth are achieved. Proper choice of transducer material and component dimensions optimizes electromechanical coupling and minimizes mechanical cross-talk and spurious low frequency lateral modes [B2], [B3-B6]. We note that the 1-3 composite exhibits ~30% higher thickness mode electromechanical coupling constant, k_{3t}, than bulk ceramic and that individual pixel k_{3t} in the 1-3 composite approaches the free k_{33} of an "ideal" long slender unconstrained piezo element [B2]. The monolithic bulk sample exhibits self-pinning and hence has $k_{3t} < k_{33}$.

B. Design of Front and Back Layers

Figure 7 is a sectional view of the array configuration along with front and back impedance-matching layers. The transducer's front surface is interfaced with a uniform $\lambda/4$ impedance-matching front layer. A patterned composite backing layer of polymer and microfabricated ceramic pillars [B7] can provide the piezoelements with the appropriate matching mechanical impedance, thus allowing its broadband operation with minimal signal degradation. The backing layer is patterned to match the active elements of the transducer. The material in the backing layer, which is between the positions of the operative piezo-elements is made of a compliant material (such as polyurethane) so as to maintain the mechanical independence of the individual ceramic elements.

The $\lambda/4$ plate, covering the front surface of the metallized transducer, can be fabricated from a composite material. Commercial impedance matching materials such as carbon and glass filled phenolic or silver-filled epoxy are available and can be machined to the appropriate thickness and glued in place. The patterned back layer can be constructed from a matching inactive array obtained from the same 1-3 composite supplier. The back layer microfabrication process will then consist of inserting conducting paths alongside the matching pillars or columns. They provide connection from the metallized electrodes to the commercial multiplexer boards.

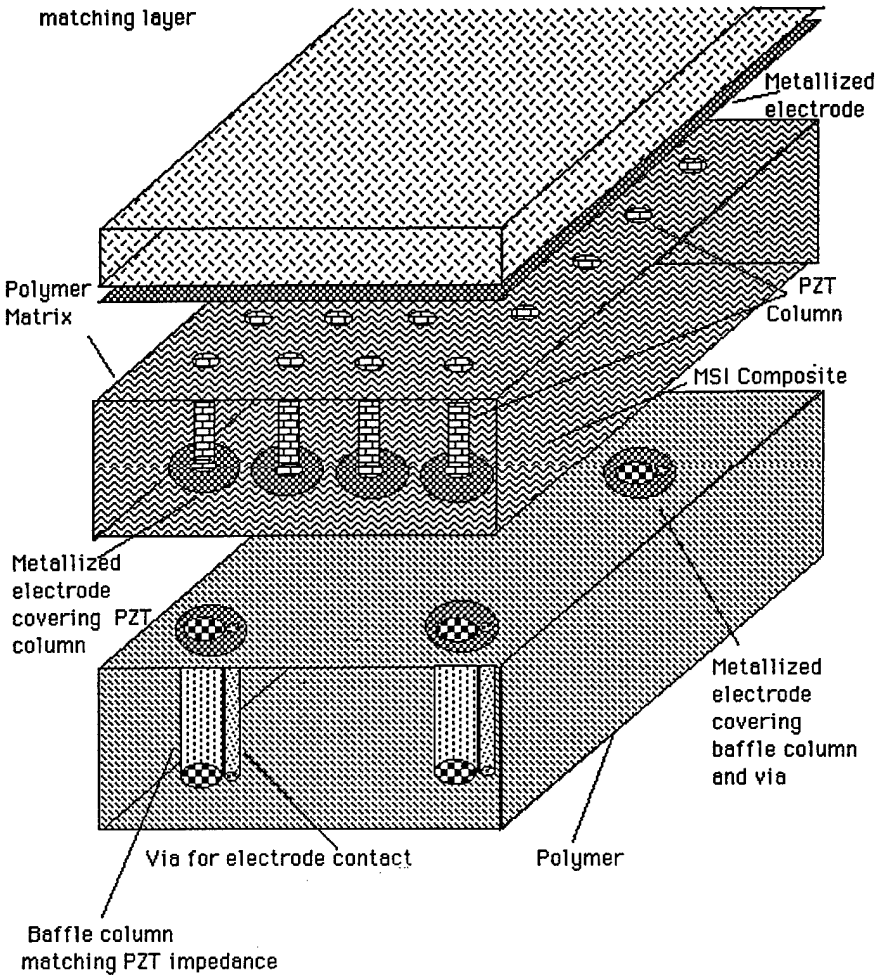

Fig. 7
Sectional view of array configuration plus front and back impedance matching layers.

C. Fabrication of the Array

Our fabrication of the array with a front layer and a back layer were done in a sequence of prototypes. Our first one was the array with back electrodes and ground plane metalization. The next step took this same first prototype and glued a quarter wavelength matching front layer made of silver-filled epoxy to the gold ground metalization. The final step will add a matching back layer with patterned conductive vias behind the transducer layer. Electronic and acoustic testing has been performed at each stage. A notable change in the SNR should be evident.

D. PZT Composite Materials and Metallization

We have developed the procedures for making the final transducer array package by a series of steps. The arrays utilize PZT piezoelectric ceramic-polymer 1-3 composite materials obtained from Materials Systems,

Inc.(MSI) [B1]. Our design utilizes the MSI periodic arrays of ceramic rods within a polymer matrix to construct a 2-D array with element size 0.75λ and element spacing 0.5λ (see Figure 8). The array materials were obtained as 2.5 cm x 2.5 cm modules. Using DC Gold Sputtering metalization, carried out in the Dental School facilities of the University of Pennsylvania, electrodes were applied to the entire front surface to serve as the ground plane. DC Sputtering, which occurs at room temperature, was used because the polyurethane (which holds together the piezo rod array) swells at temperatures above 100 degrees Celsius. This was deduced from our previous preliminary array with only 12 transducers which resulted with an open circuit on the ground plane. The thin electrode of about 300 angstroms of gold was thickened through Gold Electroplating at 65 degree Celsius, so as to have at least 1000 angstroms of Gold. The non-grounded plane of the array had individual contacts on selected array elements. These contacts were manually painted silver epoxy pads which matched the silver epoxy that was used to bond the individual wires to the pads.

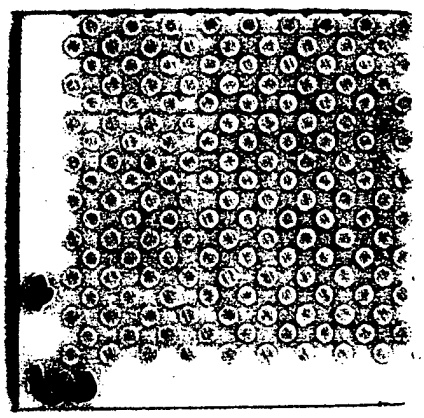

Figure 8. 2.5 cm x 2.5 cm, 1MHz transducer module. The module shown in the picture is enlarged by 2. The module consists of 306 elements.

E. Bonding and Interconnections

A 7 cm by 7 cm PC board with 40 microns of copper metalization on both sides was used to provide mechanical support to the individual connections of selected array elements. From the PC board soldered wires were connected to the array of piezo rods (see Figure 9). Since the piezo-composite fabrication process of MSI yielded a quasi-periodic element arrangement, the photolithographic process masks for the etching of the copper metalization of the PC board were obtained from digitizing actual piezo-composite array photos [B9], â technique we have used in the past. This allowed for ohmic patterns which correspond to the piezo rods. The copper pattern on the front side of the PC Board consists of .5 mm squares (which locations correspond to the piezo rods) with lines to pads (which correspond to a 54 pin socket). The design of the ohmic lines, not including the contacts for the pin socket, can be seen on Figure 9. The side view of the copper pattern and its location on one side of the PC board can be seen on Figure 10. The squares have 0.25 mm holes which are filled with a copper wire (0.13mm in diameter) which stick out to a length which would contact the piezo rods. The only copper pads that do not have lines are four center elements which are to be connected to individual copper wires. On the backside of the board (see Figure 10, #5) there are: a copper pattern, spacers, and locating pins. The copper pattern, which consists of filled in circles (which was possible with the digitized picture of the

piezo rods and photolithographic processes), served as additional support for the wires of center receiving elements and for wires that needed solder repair, more accurate positioning of the locating pins, and visual confirmation that the wires would accurately connect to a piezo rod. Spacers were soldered wires which provide evenly spaced pressure points needed when connecting the board to the array. Locating pins are soldered copper wires (0.8mm in diameter) into 1.1 mm holes on the PC board. The array has six matching holes corresponding to the farthest elements from the center which are not in use. (See Figure 11 for the cross section view of array assembly.)

F. Electronic Connections

There were 54 receiving elements which were connected to a pin socket. Four transmitting elements were chosen from the center. These had individual wires which plug into a contact to a coaxial cable.

G. Transducer Array Testing and Electrical Testing

Selected elements of the array were characterized throughout the design process to provide data for optimization of interfacing between the active piezoelectric elements and the first stage of electronics. These measured characteristics are important as the overall performance of the imaging system is crucially dependent on the sensitivity of the front-end design and its SNR.

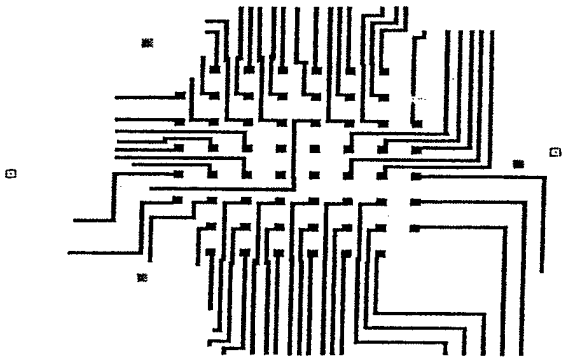

Figure 9. The array of squares connected to lines are the receiving elements. The four center squares without lines are transmitting elements. Six of the surrounding squares without lines are locations of the position pins.

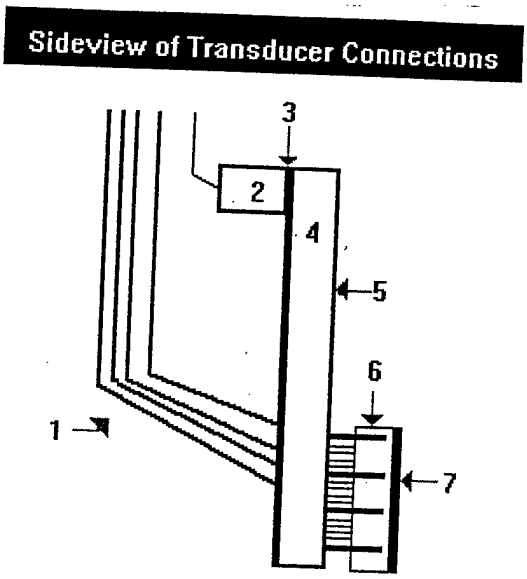

Figure 10. The ohmic contacts for the individual elements are illustrated by the above picture and the below description. 1. four wires to transmitting transducers. 2. 54 pin socket. 3. copper pattern on the PC board. 4. PC board with wires, spacers and locating pins. 5. backside of PC board. 6. array holes for 6 locating pins. 7. ground metalization side of array.

Optimization of SNR involves knowledge of the piezoelectric element impedance and information on the possible changes in the impedance due to ohmic contacts of the piezoelectric structure using different auxiliary materials. Similar measurements should also be made for the final array prototype with selected individual elements appropriately connected.

On an Impedance Meter each of the 57 elements were tested for impedance from 0.1 to 19.6 kHz in increments of 0.5 kHz. 52 (3 transmitting and 49 receiving) elements demonstrated uniform impedance ranging from 9.77 to 0.341 Mohms(see Figure 12). One of the 57 elements served as a control for bad contacts, because it did not have a wire connecting from the PC board to the array. Four transducers had high impedance similar to the control (e.g. at 10kHz ranging from 2.2 to 13Mohms). Thus it can be deduced that the difference in impedance is due to bad contacts on the wire. Of the intended 57 total elements, 52 proved to have good contacts. The average capacitance was 23.1 pF.

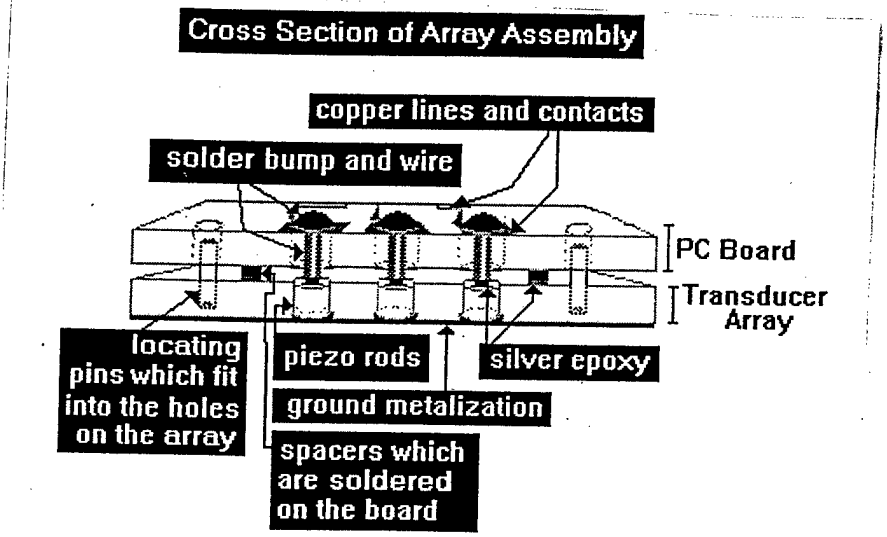

Figure 11. The array assembly consists of a PC board with copper wires soldered to copper contacts, soldered spacers and soldered locating pins. On the top side of the PC board are copper contacts and lines that lead to a 54 pin socket. Locating pins fit into holes in the array. Copper wires are bonded to the rod metalization with silver epoxy. Spacers prevent bent wires and short circuits and bond to the array with silver epoxy for mechanical support.

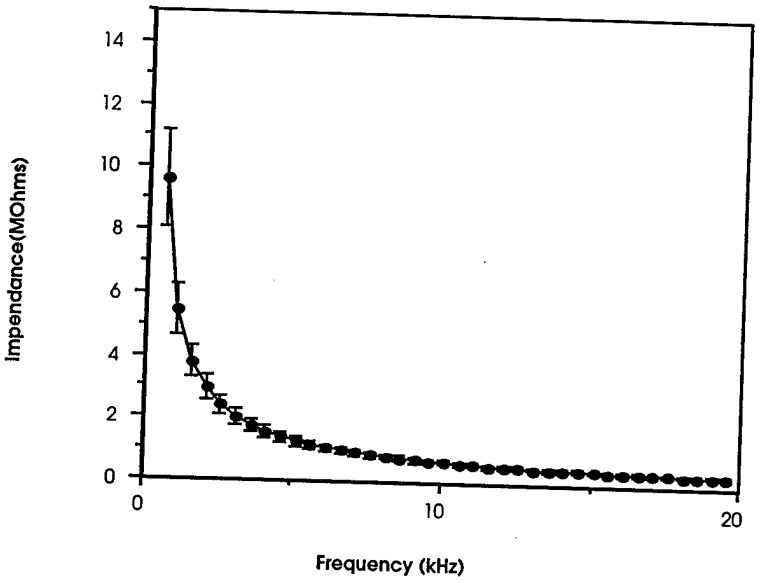

Figure 12. The impedance (1/ljwCl) of 52 out of 57 elements were uniform and of the order of Mohms (<0.4Mohm for f>20kHz). The standard deviation is drawn by error bars.

H. Acoustic Testing

Figure 13 is a block diagram of our water tank testing system. The first tests were made in transmission, where each selected transducer element acts as a transmitter and a needle hydrophone (0.6 mm in diameter) as a receiver. An ultrasound pulser (Reflectoscope) generates RF pulses that drive the selected element one at a time. The received RF signals are amplified by the low noise preamp and amp inside the pulser. A digital scope (Tek 2230) samples the 16 bit RF data at 500 MHz which is well above the Nyquist frequency. The digital data are transferred to PC through a GPIB board.

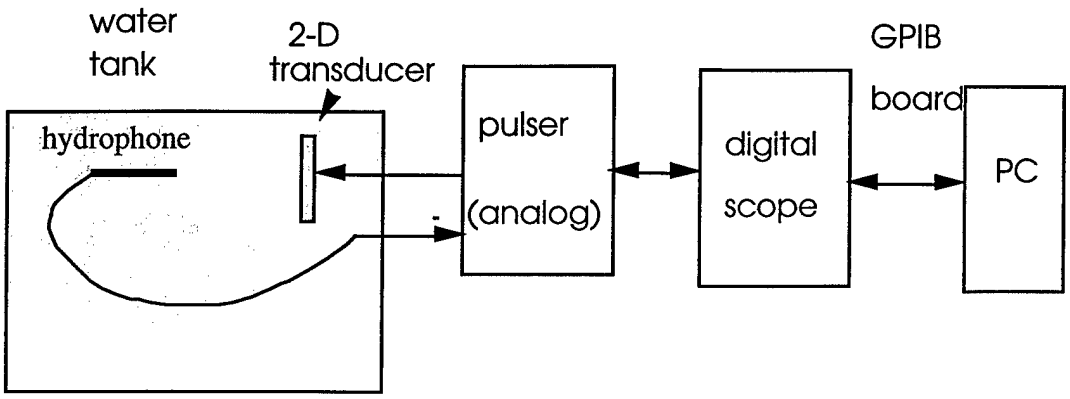

Figure 13. Block diagram of water tank testing system.

Figure 14 is a typical impulse response of a single element without front and back layers. The SNR is 24 dB which is very good. SNR should be further improved when the front and back layers are added to the transducer layer.

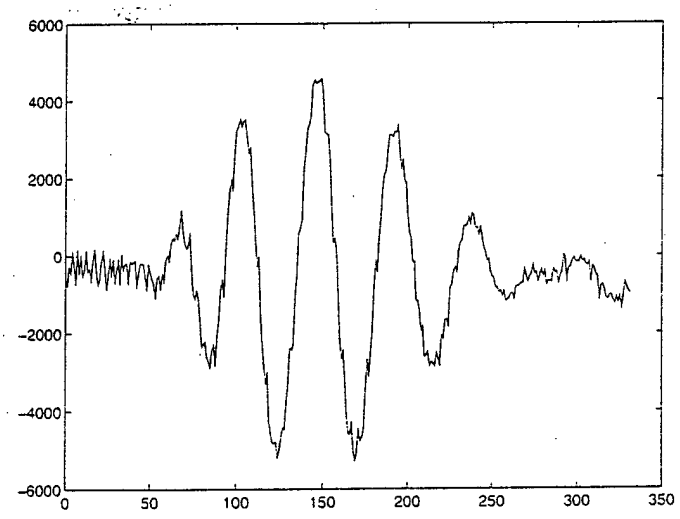

Figure 14. Impulse response of a single element.

I. Summary

From this preliminary prototype we deduced that the patterned PC board with soldered wires worked as a good mechanical support of ohmic lines and provided accurate contact. The next step involves using this same prototype at first, however, a back layer will be added to the transducer layer. A quarter wavelength front layer has been glued to the transducer array twice but the contact was not very good. We need to reglue the front layer with good contact. The final electronic and acoustic testing of the array will be completed after the front and back layers are in place. After the completion of electric and acoustic testing of the 1MHZ array, we will have complete knowledge about array fabrication procedures and pitfalls. Our next milestone is the development of a 3.75 MHz, 0.75 wavelength array with an element size of 0.3 mm. This frequency is suitable for breast imaging.

6.2.2. A simple 2-D ultrasound array

To serve our immediate need of a 2-D ultrasound array, we have built a simple array made of multiple commercial crystals. Since the crystals are small (1.5 mm in diameter), they can be used as an array when the crystals are distributed over the desired surface (see Figure 15a). The resolution of the array is not high due to the sparse quality of the array but it is adequate to demonstrate the principles.

A. Array

Each ultrasound PZT crystal works in pulse-echo mode; i.e., it transmits and receives ultrasound pulses. The central frequency of the crystal is 5 MHz and the bandwidth is about 50% (Ultra Laboratories) . The diameter of the crystal is 1.5 mm and the outer diameter including the shell is 2.5 mm. The 3dB beamwidth of the crystal is approximately λ /d. At a wavelength (λ) of 0.3mm and a diameter (d) of 1.5mm, each crystal's transmitted beam forms an 11.5^{o} cone. The crystals were spaced by 4 mm in both x and y directions. This spacing compromises the field of view and resolution. With the array configuration shown in Figure 15, the beams of nearest neighbor elements overlap and they are used to form the transmitted and received beams. The nearest neighbor elements of transducer **x** is illustrated by the dashed rectangle in the figure. A total of 20 receiving beams steered straight ahead were formed and no beam steering was used in image formation due to the sparse quality of the array. Therefore, the field of view is restricted to 16 mm by 20 mm.

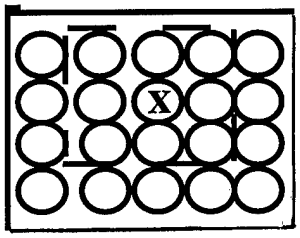

Figure 15. Geometric configuration of the 20-element crystal array. The horizatal dimention of the array is 20 mm and vertical dimention is 16mm.

B. Front end Electronic System

Figure 16 shows a diagram of the ultrasound data acquisition system. During data acquisition, the pulser (Sperry) generates one cycle short RF pulse of 120 volts peak that drives one crystal at a time selected by a 20:1 high voltage multiplexer board (Matrix Cop.). The multiplexer is controlled by a PC through its serial port. The RF signals returned are received by one selected crystal at a time and are amplified by a low noise preamp (AD604, Analog Devices) connected to the short cable of the crystal. AD 604 is a TGC amplifier and a fixed gain is used in our experiments. The pre-amplified signals are multiplexed by another 20:1 multiplex board consisting of two 16-channel CMOS multiplexers, and are amplified by a second stage AD 604. The gain of this AD 604 can be controlled. Low noise preamplifiers connected to the cables of the crystal transducers before the multiplexer board significantly improves the signal-to-noise ratio. The amplified signals are digitized by a PC A/D scope board (Gage Applied Inc) at a sampling rate of 40 MHz with an 8 Bit analog-to-digital converter. This sampling rate is about four times the highest frequency component of the transmitted pulse. Measurements obtained from all nearest neighbor transmission and reception positions are used to form volumetric B-scan images. A sequence of 2-D x-y image slices is formed by summing up the evolve detected

signals within consecutive ranges. The slice thickness used in the experiments varies from 2 mm to 3.3 mm in range.

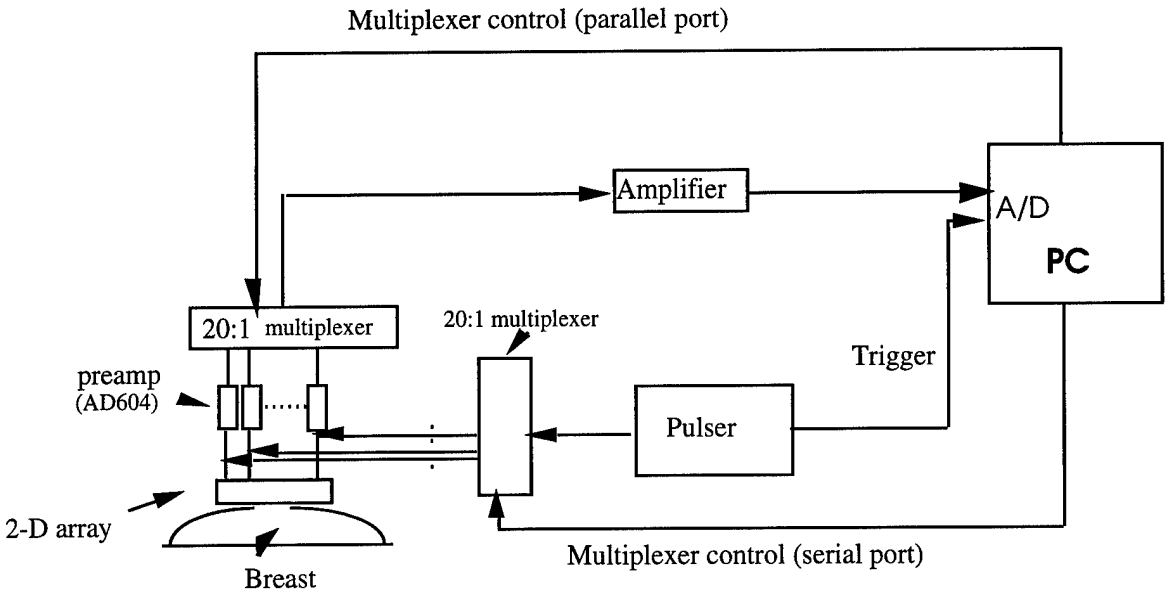

Figure 16. Electronic configuration of the ultrasound data acquisition system. Preamps are connected to the short cables of 20 crystals. Transmission is controlled by a high voltage multiplexer to drive one crystal at a time. Received signals are amplified by the preamps and switched by another 20:1 multiplexer board. The selected channel is amplified by the second stage amplifier and the received signal is sampled by a high speed A/D board.

C. Results

The imaging resolution of the array has been tested in a water tank using various testing targets. The targets are bars and balls with well defined geometries. Figure 17a is the spatial image of a plastic bar (4.5 mm in diameter). The testing configuration is shown in Figure 17b. One end of the bar is facing the 2-D transducer head. Since the resolution size of the image is about 4mm, this end of the bar is imaged correctly as an approximately 4 mm x 4 mm rectangle.

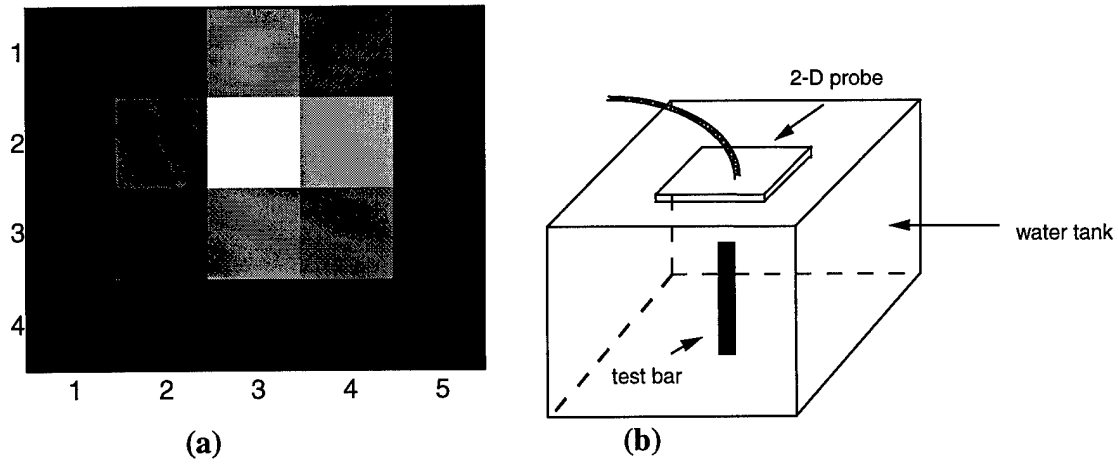

Figure 17. (a). A spatial image of the plastic bar with one end of the bar facing the array head. (b) Testing configuration.

We have implemented the phase deaberration algorithms and TIF in this 2-D imaging system.

6.3. Novel combined ultrasound and near infrared optical imaging

6.3.1. Combination of ultrasound with NIR cancellation technique

Optical phased array

An approach to localization for NIR detection is given by Chance, et al. [C23-C24]. In their method, a simple optical phased array system (OPAS) for object positioning has been constructed that measures the interference of intensity-modulated NIR diffuse light signals (in-phase, 0^o, and out-of-phase, 180^o) at detector positions equidistant from two spatially separated sources. In the absence of heterogeneity's (Figure 18a) the signals will cancel at locations equidistant from the two sources. The null plane or line is always at the bisecting plane or line, and the deviation between null and bisecting lines is zero. *In vivo* experiments have demonstrated clear-cut amplitude nulls and sharp phase transitions [C23]. If a heterogeneity is present in the medium (Figure 18b), the balance of the source waves on the bisecting line is perturbed and the null line will deviate. This deviation is used as an indicator in the scanner to detect an inhomogeneous object with respect to a homogeneous background. The line of sight of the heterogeneity is obtained from the newly formed null line through either mechanical or electronic scanning (Figure 18c). However the position of the heterogeneity is only known to lie somewhere near the null plane. Another source and equidistant detector pair deployed from a different direction could provide an additional null line, and two lines of sight could be used to locate the heterogeneity. More recently, the same group has extended the one-dimensional (1-D) cancellation system into a two-dimensional (2-D) cancellation system [C24]. Ten pairs of equidistant detectors and nine laser diode sources were mounted in a 10 x 10 cm^2 rubber pad which was hand-held against an examined breast with the patient in a supine position. Multiple null lines were generated from all possible pairs of source and equidistant detectors. From these multiple null lines, the spatial location of a heterogeneity can be detected. Imaging, referred to as null imaging in the following text, has been performed by processing the measured amplitude and/or phase signals using a back-projection algorithm. In addition to localization of the heterogeneity, this method can also provide deoxygenation information on the detected target when dual wavelengths are used, for example, 760 nm and 830 nm . The deoxygenation image is obtained from the difference between two null images obtained at these two wavelengths. Note that the absorption spectra of oxyhemoglobin and deoxyhemoglobin are quite different at 760 nm and 830 nm and the maximal differences are at these two wavelengths. Furthermore, the target blood volume image can be well approximated by the weighted sum of the null images at the two wavelengths. More than 50 patients have been studied so far. Using maximum changes of blood volume and deoxygenation as criteria and biopsy results as the "gold" standard, the malignant tumors were well separated from the benign masses and cysts. The maximum changes were measured in the lesion regions relative to background tissue. Thus this method has merit in breast cancer detection. However, the resolution of null imaging is very low, and exact object shape and size information cannot be obtained.

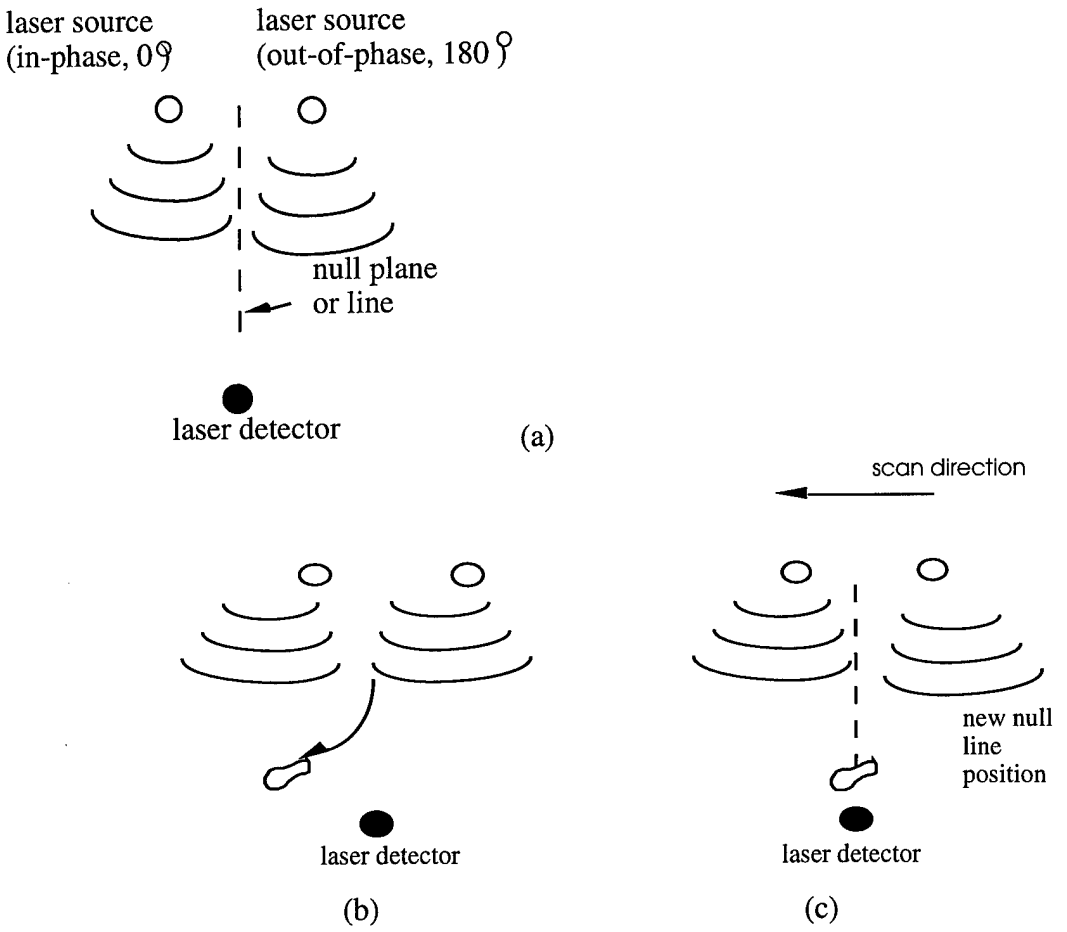

Fig.18. Illustration of object detection by the optical phased array positioner. (a) Null line position when no heterogeneity is present. (b) Null line is deviated toward the heterogeneity . (c) New null line is formed at the object line-of-sight through scanning.

Combined array and imaging

A novel combination of the two suboptimal systems, namely ultrasound and OPAS, as reported in [C32], has shown a superior performance in detection sensitivity and specificity compared with ultrasound alone in phantom studies. Since commercial ultrasound scanners use 1-D transducer arrays, the combination has been implemented in one dimension by coaxially mounting a 1-D ultrasound probe with a 1-D OPAS. The combination took advantage of ultrasound imaging and OPAS localization capabilities, and directed human observers to look for possible targets and lesions within a ROI in the co-registered ultrasound images. The ROI was determined from highly sensitive optical line-of-sight information. As a result, the detection sensitivity and specificity of a few mm object buried in a scattering phantom has been improved significantly. Experimental set-ups, examples and statistics are described in the following paragraphs.

In our phantom studies [C32], we incorporated the simple NIR positioner into an ultrasound imaging system (Figure 19). An ultrasound phased array probe is coaxially mounted with the two laser diode sources, referred to as the coaxial probe in the figure, and the coaxial probe and the optical detector assembly are mechanically translated together on a rigid frame by a stepping motor. This simple

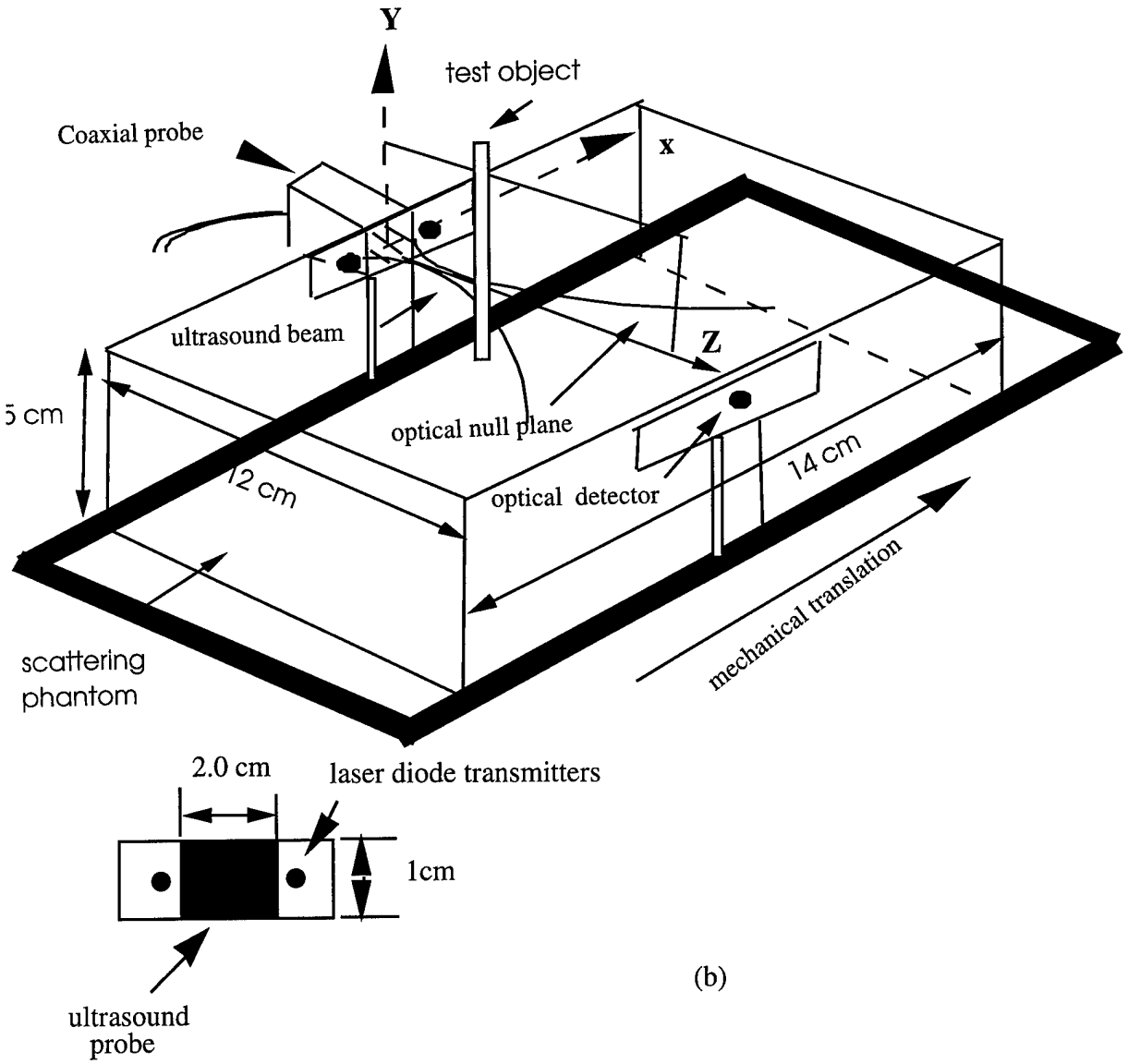

Figure 19. (a) Coaxial ultrasound and optical probe and optical detector assembly. The coaxial probe and detector assembly is mechanically translated by a stepping motor (not shown). The scattering phantom is fixed on the floor. The dimension of the scattering phantom is 7.5 x 12 x 14 cm. The ultrasound beam is in X-Z plane and optical null plane is in X-Y plane. A cylindrical-like object is inserted along Y direction. (b) front view of the coaxial probe.

combined system was tested using models consisting of a single simulated tumor of a few mm size buried in a scattering phantom. The homogeneous scattering phantom was made of an acrylamide gel (7.5 x 12 x 14 cm^3), and scattering particles at optical and ultrasound wavelength scales were added to the acrylamide solution before the gel was formed. In each test, the combined system was mechanically translated to scan for the small object. In a typical experiment, 1 mm step size was used. At each scanning position, optical amplitude and phase data and an ultrasound sector scan image were acquired. The object line-of-sight information was obtained from the optical data and was coded into ultrasound images after scanning. A total of 30 targets with various acoustic and optical absorption and scattering properties were studied, and ultrasound images without and with line-of-sight information were graded

for the presence of lesions on a five-point scale (see Table I) by two experienced radiologists in the Breast Imaging Section of the Radiology Department of the University of Pennsylvania. A typical example of optical scanning and ultrasound image evaluation is demonstrated as follows.

Table I. Evaluation form

Please check for possible lesions or targets.

Target #1
1. No lesion or target present
2. Probably no lesion or target present
3. Lesion or target may be present
4. Lesion or target probably present
5. Lesion or target definitely present

Target #2
1. No lesion or target present
2. Probably no lesion or target present
3. Lesion or target may be present
4. Lesion or target probably present
5. Lesion or target definitely present

Target #3...
Target #4...
Lesions, or targets may be hyperechogenic or hypoechogenic. If you identify any lesions please circle and number them on images.

Figure 20 shows optical amplitude and phase responses when concentric black-plastic tubes of 1.9 and 1.7 mm diameters filled with 0.5% intralipid (optical scattering medium) were inserted into the scattering phantom at approximately 6 cm depth. The black testing object is an optical absorber which also generates an inhomogeneous ultrasound echotexture (see Figure 21) as some tumors may do. The inhomogeneous echotexture is produced by the concentric tubes. The sharp phase transition and amplitude null correspond to the object line-of-sight. As a result of mechanical translation, a sequence of ultrasound images was obtained. Since weak targets in a sequence of images were more readily detected than in a single image, triple images taken in 1 mm steps at the neighborhood of the optical phase transition and amplitude null were selected in each test. The criteria of triple image selection are described in detail in [C32]. Since the optical assembly and ultrasound probe are coaxially mounted, the object in the triple images always appears along the ultrasound scan axis. To avoid giving any prior knowledge to human observers about the object location, we chose different image windows in different tests to randomize the object location. In each test, the image windows used for triple images were the same and the object position shift was caused by the 1 mm lateral translation of the imaging system. In this example, three images taken at phase transition and amplitude null positions (16, 17, 18 mm) are shown in Figure 21. The image of the object, indicated by an arrow, is highly obscured by speckle noise. Two observers evaluated the triple image using the form given in Table I. They were told that they could mentally average these images to filter out artifacts and noise. One observer picked up the target and marked category 4 on the evaluation form. When the same images coded with optical line-of-sight information, shown by dashed lines in Figure 22, were presented to the observer, his detection

confidence increased from category 4 to 5. Another observer completely missed the target in ultrasound-alone images and marked category 1 on the form. When the images with object line-of sight information were presented, the second observer picked up the target and selected category 3 on the form. This example shows the improvement in detection sensitivity when the combined method is used.

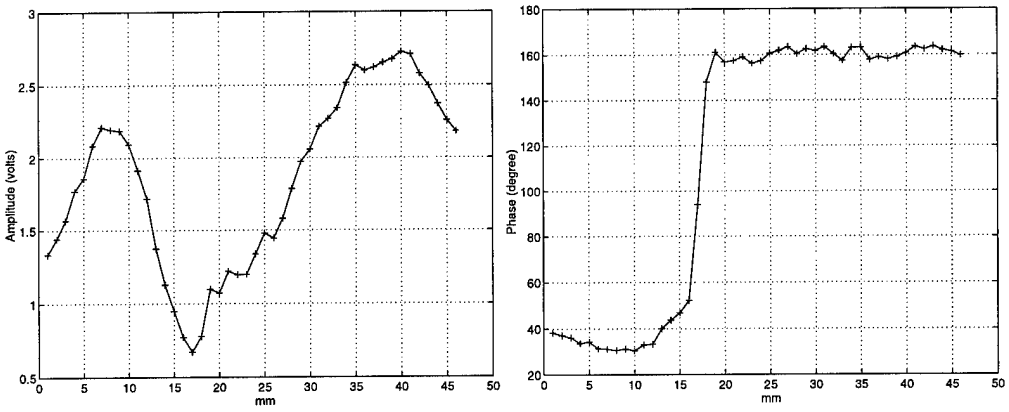

(a) (b)

Figure.20. Optical response when concentric black plastic tubes of 1.9 and 1.7 mm diameters filled with 0.5% intralipid were inserted into the scattering phantom. (a) Amplitude response and (b) phase response. The amplitude null and phase transition are indications of the object line-of-sight.

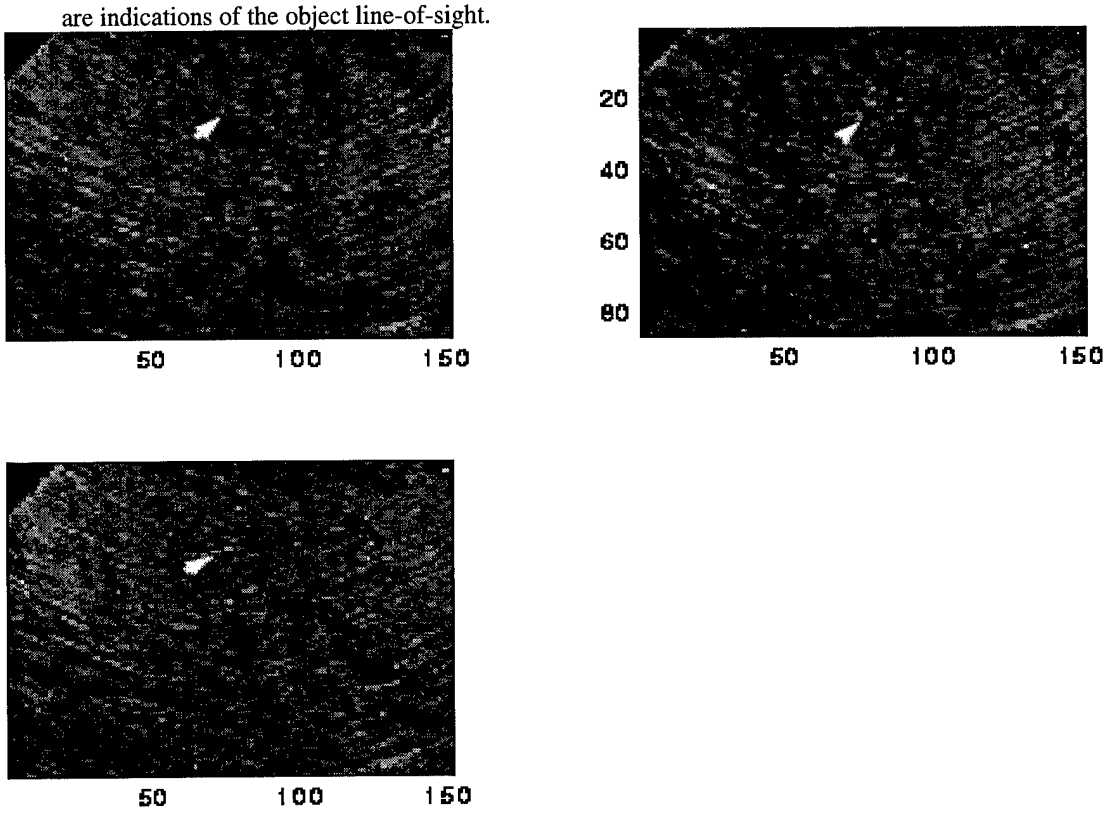

Figure 21. The triple images taken at lateral positions 16, 17, 18 mm. Target is indicated by arrow.

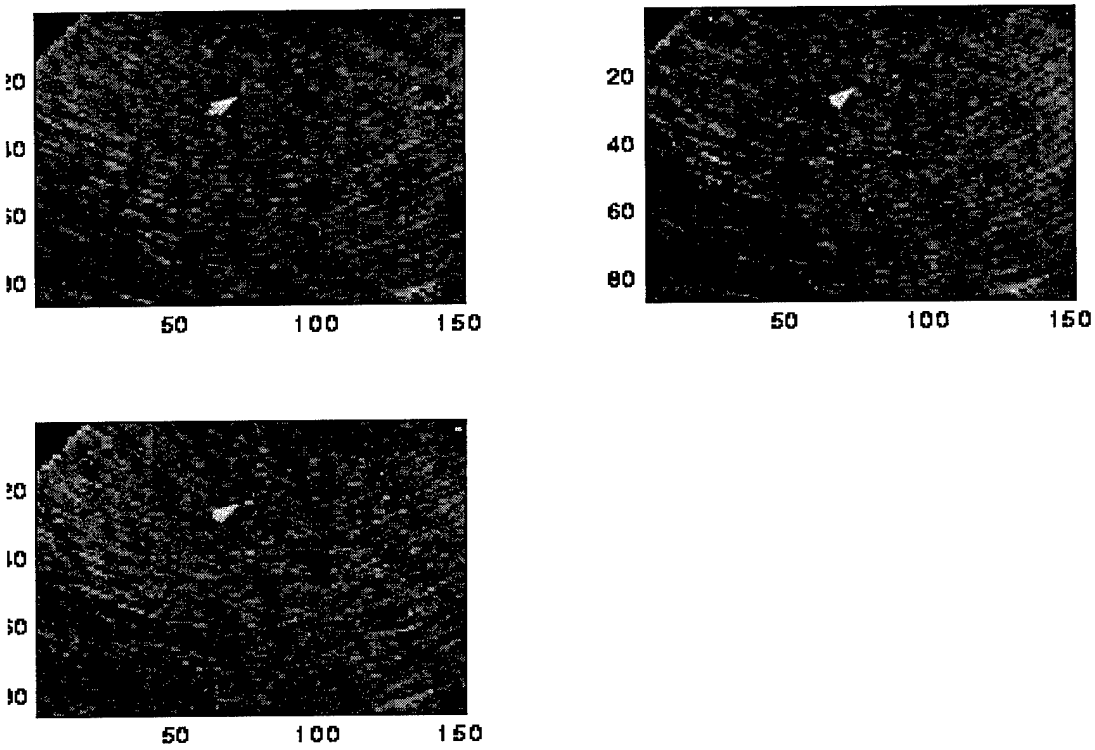

Figure 22. The same triple images as shown in Figure 20 but optical line-of-sight information was coded in the images as indicated by dashed lines. Target is indicated by arrow.

We studied a total of 30 positive trials and 21 negative trials. Average empirical ROC curves of ultrasound (solid) and ultrasound-light (dashed) of the two independent readings for the two observers are shown in Figure 23. The superior performance of ultrasound-light is shown by the higher ROC curves. The fact that ultrasound ROC curves are close to the major diagonal indicates that the detection information is very poor in this phantom study and that targets can only be recognized at a slightly better than chance level. The area under the ROC curve provides a measure of discriminatory efficacy: an area of 100% denotes an ideal system and 50% denotes an ineffective system. The calculated areas under ROC curves of ultrasound and ultrasound-light of observer #1 are 54% and 79%, respectively and of observer #2 are 50% and 86%, respectively. The mean values are 52% for ultrasound and 83% for ultrasound-light, respectively.

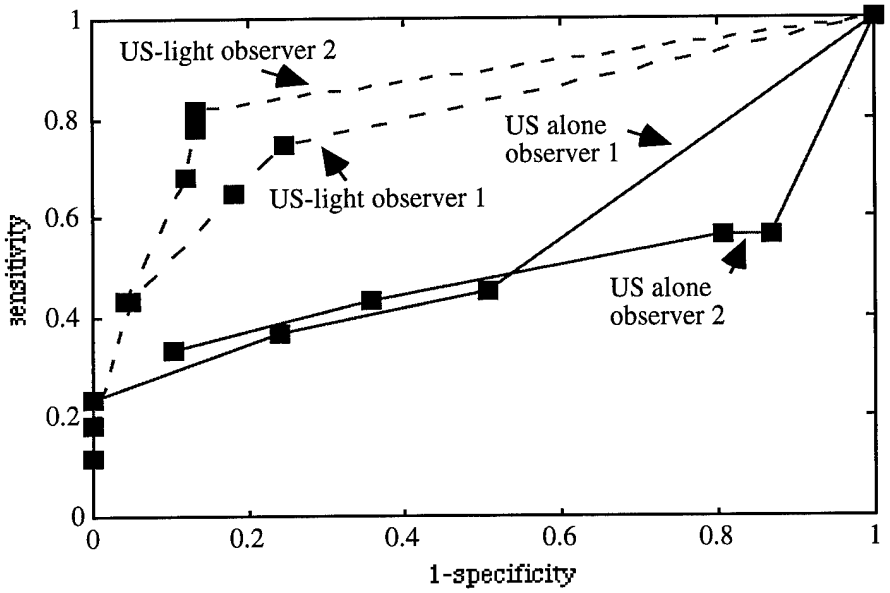

Figure 23 Average ROC curves of two readings from two observers. The ROC curves of ultrasound method are plotted in solid lines and ROC curves of ultrasound-light are plotted in dashed lines.

The model studies described in the preliminary work have been designed to understand how optical techniques can be first used to improve ultrasound detection and what influence optical ROI information will have upon ultrasound detection by human observers. The simple "two-dimensional" objects used in the studies as well as the scattering phantom in which they are embedded are obviously inadequate to reproduce all the properties of breast tumors and breast tissue. In particular, *in vitro* studies are limited because almost all biological sources of optical contrast will be lost, for example oxygenation/deoxygenation, blood volume, etc. Clinical studies are required to fully evaluate this combined imaging method.

6.3.2. Combination of ultrasound with NIR tomography technique

The studies reported in 6.3.1 used a one-dimensional combined probe with a commercial ultrasound transducer and a one-dimensional near-infrared scanner mounted co-axially. The NIR scanner provided lateral position (x) of the heterogeneity and conventional ultrasound proved x-z image of the heterogeneity, where z is the propagation direction. This choice accommodates the data acquisition requirement of current one-dimensional commercial ultrasound transducers. However, the one-dimensional optical scanner could not provide depth information of the embedded heterogeneity. Reconstruction of x-z images with optical techniques is very difficult because of the poor depth resolution associated with optical imaging (even more poor than spatial resolution). Currently, optical breast imaging can be performed by mounting multiple sources and detectors over a two-dimensional surface (2-D probe) [C30]. Measurements made at multiple source-detector positions can be used by various image reconstruction schemes to produce x-y images at slice depths underneath the probe. To accommodate optical data acquisition requirements, a two-dimensional ultrasound array with array elements deployed over the same 2-D surface is preferred. A 2-D ultrasound array can provide spatial (x-y) images of the breast at any propagation depth toward the chest wall by electronically scanning an

acoustic beam in azimuth (x) and elevation dimensions (y). Such x-y images can be used to co-register with optical images. However, 2-D ultrasound arrays are not commercially available. To demonstrate the feasibility of co-registration of ultrasound and optical images, we have conducted experiments using the simple two-dimensional ultrasound array described in Section 6.2.1 and a NIR imager borrowed from Prof. Arjun Yodh of Physics Department of the University of Pennsylvania. The combined probe consists of the 2-D ultrasound and NIR laser diode sources and avalanche photodiode (APD) light detectors (see Figure 24). The ultrasound array and NIR sensors were coaxially mounted on a firm plastic plate. The ultrasound array was located at the center and NIR sensors were distributed at the periphery. This array configuration best accommodate ultrasound coherent imaging and NIR diffusive imaging characteristics. The resolution and contrast of the ultrasound system are not the state-of-the-art because of the sparse quality of the array and because of the low sensitivity of the wideband crystals. However, with this system we can demonstrate the feasibility of co-registration. The simple 2-D ultrasound can be easily replaced by a commercial 2-D array when it is available to obtain state-of-the-art ultrasound images.

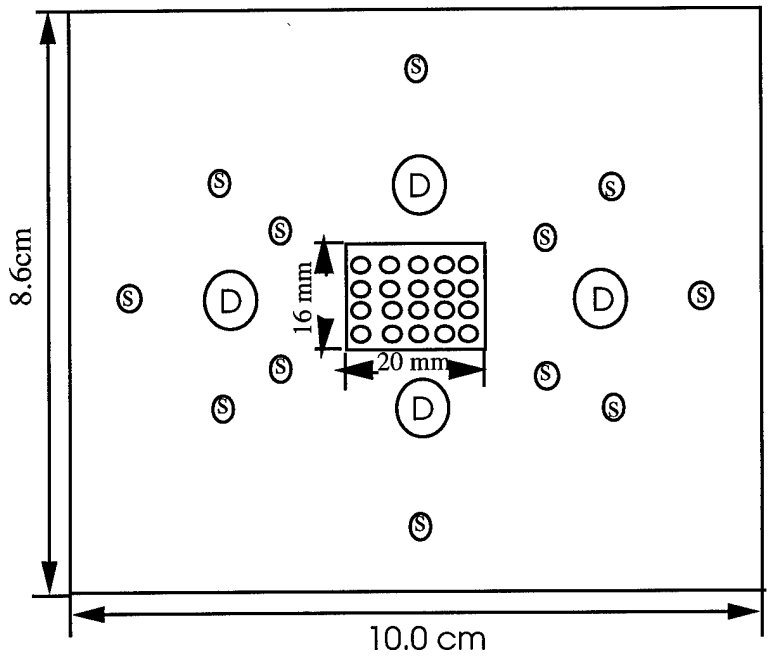

Figure 24. Geometry of the combined probe. The ultrasound crystals are located in the middle and NIR detectors (D) and laser diode sources (s) are distributed at the periphery. This array configuration best compromises the ultrasound coherent imaging and NIR diffused light imaging characteristics.

Figure 25 shows optical absorption (top) and ultrasound (bottom) images obtained from the combined probe. The image pixel size is 4 mm x 4 mm in both ultrasound and optical images. The target is a 12 mm diameter raisin sphere located at 20 mm depth. The target optical absorption coefficient is μ_a = 0.2cm^{-1} and scattering coefficient is $\mu_{s'}$=8 cm^{-1}. These optical parameters simulate tumor optical properties. The ultrasound reflectivity of the share is moderate which simulates some tumor acoustic properties. The shapes of the target in both images are congruent and locations of the target are the same. The resolution of the ultrasound image is better than that of optical image. This example demonstrates that we can obtain both acoustic and optical parameters of the target and perform detection and diagnosis based on both acoustic and optical information.

We have obtained dozes of images of various testing objects and we are analyzing the data now. This work will be reported in IEEE Ultrasonic Symposium early Oct. at Sendai Japan [C35].

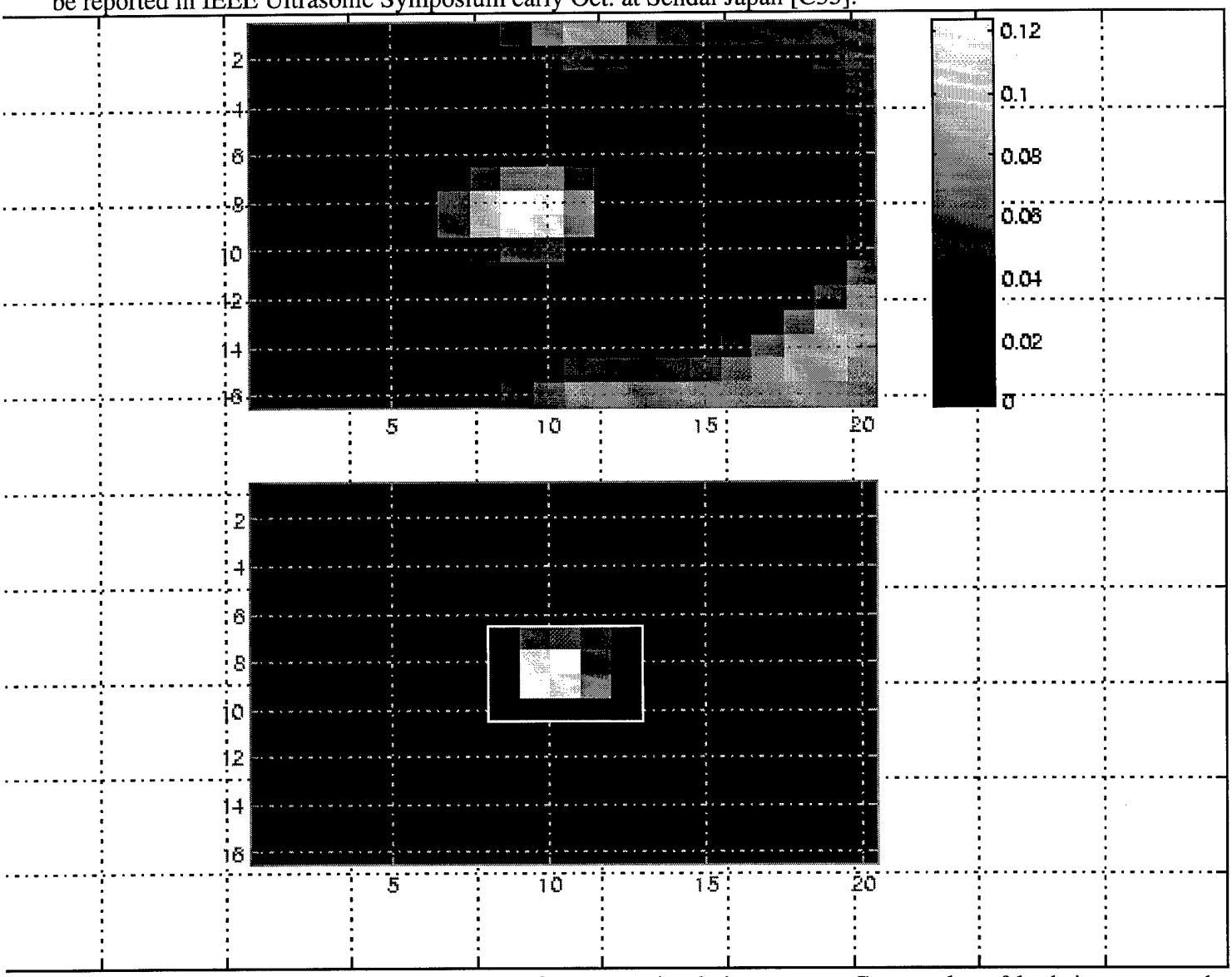

Figure 25. Optical and ultrasound images of a tumor simulating target. Gray scales of both images are the same.

7. CONCLUSIONS

In conclusion, we have developed a successful wavefront compensation algorithm (TIF) which has shown promising results in improving contrast resolution of ultrasound breast imaging.

We have constructed two prototypes of two-dimensional ultrasound arrays. From the construction of the first prototype, we have gain considerable expertise on transducer design and fabrication. The second prototype allows us to demonstrate the principle of 2-D wavefront compensation and co-registration of ultrasound and optical images.

We have developed a novel imaging technique which combines ultrasound and near infrared optical imaging methods. The preliminary results have demonstrated the potential of this method in breast cancer detection.

8. REFERENCES

[A1] Anthony Vanderlugh, "Optical Signal Processing," Chapter 5, John Wiley & Sons, Inc 1992.
[A2] Zhu, Q. and Steinberg, B.D., "Modeling and Correction of Incoherent Wavefront Distortion" Special issue of I'nal. J. Sci. Tech. Imaging, Wiley, (03) 322:335, 1997.
[A3] Zhu, Q., and Steinberg, B.D., "Deaberration of Incoherent Wavefront Distortion: An Approach Toward Inverse Filtering," IEEE Transactions on Ultrasonic, Ferroelectrics and Frequency Control, (40), No.3, 575-589, May 1997.
[A4] U.S. Patent 08881316: "System and Method for Improving Ultrasound Imaging Contrast by Amplitude Compression of Ultrasonic Wavefront Signals", by Zhu, Q. and Steinberg, B. (1997)
[A5] Hall FM, Storella JM, Silverstone DZ, et al, "Nonpalpable Breast Lesions: Recommendations for biopsy based on suspicious of carcinoma at mammography. Radiology 1988; 167:353-358.
[A6] Shtern F., Stelling C., Goldberg B., Hawkins R., "Novel Technologies in Breast Imaging: National Cancer Institute Perspective," Radiology 153-156 (1995).
[A7] Moshfeghi, M. and Waag, R.C., In Vivo and in Vitro Ultrasound Beam Distortion Measurements of a Lar Aperture and a Conventional Aperture Focused Transducer, *Ultrasound Med. Biol. 5,* 415-428 (1988).
[A8] Trahey, G.E., Freiburger, P.D., Nock, L.F., and Sullivan, D.C.,"*In Vivo* Measurements of Ultrasonic Be: Distortion in the Breast," Ultrason. Imag. 13, 71-90 (1991).
[A9] Zhu, Q. and B. D. Steinberg, "Large-Transducer Measurements of Wavefront Distortion in the Female Breas Ultrasonic Imaging **14**: 276-299 (1992).
[A10] Freiburger, P.D., Sullivan, D.C., LeBlanc, B. H., Smith, S. W., and Trahey, G.E., "Two Dimensional Ultraso Beam Distortion in the Breast: In vivo measurements and effects," Ultrason. Imag. 14(4), 398-414 (1992).
[A11] Zhu, Q., Steinberg, B. D. and Arenson, R., "Wavefront Amplitude Distortion and Image Sidelobe Levels -P II: In Vivo Experiments," IEEE Transactions on Ultrasonic, Ferroelectrics and Frequency Control (40) 754-761 (199
[A12] Hinkleman, L.M., Liu, D-L., Waag, R.C., Q. Zhu and B.D.Steinberg, "Measurement and correction of ultraso pulse distortion produced by the human breast," JASA (97) No.3, 1958-1969 (1995).
[A13] Phase Deaberration Section of IEEE Ultrasonic Symposium, pp:1353-1370 and pp:1391-1418, 1996.
[A15] Flax, S. W. and O'Donnell, M. "Phase Aberration Correction using Signals from Point Reflectors and Diffu Scatterers: Basic Principles," IEEE Trans. Ultrason. Ferroelec. Freq. Cont., **35**(6):758-767, Nov. 1988.
[A16] Nock, L., Trahey, G. E., and Smith, S.W., "Phase Aberration Correction in Medical Ultrasound Using Specl Brightness as a Quality Factor," J. Acoust. Soc. Am., **85**(5) 1819-1833 (1989).
[A17] Attia, E.H. and Steinberg,B.D. (1989), "Self-Cohering Large Antenna Arrays Using the Spatial Correlati Properties of Radar Clutter," IEEE Trans. Antennas Prop., AP-37(1), 30-38 .
[A18] Ishimaru, A. (1978),*Wave Propagation and Scattering in Random Media*, Academic Press, New York.
[A24] Fink, M., "Time reversal of ultrasonic fields – part I: basic principles," IEEE Trans. Ultrason. Ferroelec. Fr Contr., vol. 39, pp. 555-566, 1992.
[A25] J.-L. Thomas and M.A. Fink, "Ultrasonic Beam Focusing Through Tissue Inhomogeneities with a Ti Reversal Mirror: Application to Transskull Therapy, IEEE Trans. Ultrason., Ferroelec. Freq. Contr.,Vol. 43, No 1122-1129, 1996.

[A26] Liu D-L and Waag, R.C., "Correction of Ultrasonic Wavefront Distortion Using Backpropagation and Reference Waveform Method for Time-shift Compensation," J. Acoust. Soc. Am. 96, 649-660 (1994).
[A27] P-C Li, S. W. Flax, E. S. Ebbini, and M. O'Donnell,"Blocked Element Compensation in Phased Array Imaging," IEEE Trans. Ultrason., Ferroelec. Freq. Contr.,Vol. 40, No.4, 283-292, July 1997.
[A28] S. Krishnan, Li P-C and M. O'Donnell, "Adaptive Compensation of Phase and Magnitude Aberrations," IEEE Trans. Ultrason., Ferroelec. Freq. Contr.,Vol. 43, No.1, 44-55, January 1996.
[A29] S. Krishnan, K.W. Rigby and M. O'Donnell, "Adaptive Aberration Correction Using PARCA," 1996 Ultrasonic Symp. 1363-1366.
[A30] Steinberg,B.D, "Radar Imaging from a Distorted Array: The Radio Camera Algorithm and Experiments," IEE Trans. Antennas Propag., **AP-29**(5) 740-748 (Sept. 1981).
[A31] Zhu, Q, "Ultrasonic Wavefront Distortion Compensation in Pulse-Echo Using Toward Inverse Filteri Technique," AIUM 42 Convention, March 1998, Boston (abstract number #8168).
[A32] S. Krishnan, K.W. Rigby and M. O'Donnell., "Improved Estimation of Phase Aberration Profiles," IEEE Trans. Ultrason., Ferroelec. Freq. Contr.,Vol. 44, No.3, 701-713, May 1997.

[B1] Bowen, L.J., Gentilman, R.L., Pham, H.T., Fiore, D.F., and French, K.W., "Injection Molded Fine-Scale Piezoelectric Composite Transducers," IEEE Ultrasonics Sympos. Proc., 499-503 (1993).
[B2] Oakley, C.G., "Design Considerations for 1-3 Composites Used in Transducers for Medical Ultrasonic Imaging," *Proc. of the IEEE 6th Internat. Symp. on the Applic. of Ferroelectrics*, 233-236 (1991).
[B3] Auld, B.A., "High Frequency Piezoelectric Resonators," *Proc. of the IEEE 6th Internat. Symp. on the Applic. of Ferroelectrics*, 288-295 (1986).
[B4] Gururaja, T.R., Schulze, W.A., Cross, L.E., Newnham, R.E., Auld, B.A., and Wang, Y.J., "Piezoelectric Composite Materials for Ultrasonic Transducer Applications. Part I: Resonant Modes of Vibration of PZT Rod-Polymer Composites," *IEEE Transac. on Sonics and Ultras.*, SU-32, 481-498 (1985a).
[B5] Gururaja, T.R., Schulze, W.A., Cross, L.E., Newnham, R.E., "Piezoelectric Composite Materials for Ultrasonic Transducer Applications. Part II: Evaluation of Ultrasonic Medical Applications," *IEEE Transac. on Sonics and Ultras.*, SU-32, 499-513 (1985b).
[B6] Smith, S.W., Trahey, G.E., and von Ramm, O.T., "Two-dimensional arrays for medical ultrasound," Ultrasonic Imaging 14, 213-233 (1992).
[B7] Smela, Elizabeth, PhD Dissertation, University of Pennsylvania (1992).
[8] Yin, Xiaoquing, PhD Dissertation, University of Pennsylvania (1995).
[B9] Davidsen, R. E., J.A. Jensen, and S. W. Smith,"Two-Dimensional Random Arrays for Real Time Volumetric Imaging," Ultrasonic Imaging 16, 143-163, (1994).
[B10] Schlaberg, H.I.and Duffy, J.S., "Piezoelectric Polymer Composite Arrays for Ultrasonic Medical Imaging Applications," *Sensors and Actuators, A.* (1994).

[C1] Sickles EA, "Detection and Diagnosis of breast cancer with mammography," Perspect Radiology, 1988; 1:36-65.
[C2] Dam PAV, Goethem MLAV, Kersschot E, Vervliet JV, et al., "Palpable Solid Breast Masses: Retrospective Single-and Multimodality Evaluation of 201 Lesions," Radiology 1988; 166:435-439.
[C3] Paramagul C, Helvie MA, Adler DD,"Invasive Lobular Carcinoma: Sonographic Appearance and Role of Sonography in Improving Diagnostic Sensitivity, Radiology 231-234, 1995.
[C4] Sickles EA, Filly RA, Callen PW, "Benign breast lesions:ultrasound detection and diagnosis, "Radiology 1984; 151:467-470.

[C5] Kopans DB, Meyer JE, Lindfors KK, "Whole-breast US imaging:four-year follow-up." Radiology 1985; 157:505-507.

[C7] Stavros TA, Thickman D, Rapp C, "Solid breast nodules: Use of sonography to distinguish between benign and malignant lesions," Radiology 1995; 196: 123-134.

[C8] Yodh A and Chance B,"Spectroscopy and imaging with diffusing light," Physics Today, March 1995.

[C9] SPIE Proceedings of Optical Tomography and Spectroscopy of Tissue: Theory, Instrumentation, Model, and Human Studies II (1997), edited by Britton Chance and Robert R. Alfano.

[C10] Beauvoit B, Kitai T. and Chance B,"Contribution of the Mitochondrial compartment to the optical properties of the rat liver," Biophysical Journal Vol 67, pp2501-2510 (1994).

[C11] Folkman J," Introduction: angiogensis and cancer," Cancer Biology 1992; 3:47-71.

[C12] O'Leary M. A, Boas D A, Chance B and Yodh AG,"Reradiation and Imaging of Diffuse Photon Density Waves Using Fluorescent Inhomogeneities," Journal of Luminescence, Vol. 60-61, PP. 281-286, 1994.

[C13] Franceschini, M.A., Moesta, K.T., Fantini, S., Gaida, G., Gratton, E., Jess, H.,Seeber, M., Schlag, P.M.,Kashke, M.,"Frequency-domain techniques enhance optical mammography: initial clinical results, Proc. Of Nat. Ac. of Sci., Vol. 94, pp. 6468-6473 (June 1997).

[C14] Fantini, S., Franceschini, M.A., Gaida, G., Gratton, E., Jess, H., Mantulin, W,M., Moesta, K.T., Schlag, P.M., and Kashke, M.,"Frequency-domain optical mammography: Edge effect corrections, Med. Phys. 23, 1-9 (1996).

[C15] Arridge, S. R., in Medical Optical Tomography:Functional Imaging and Monitoring, ed. G.Muller et al., SPIE Optical Engineering Press, Bellignham, WA, Vol. IS11, 31-64 (1993).

[C16] O'Leary, M. A., Boas, D. A., Chance, B. and Yodh, A. G., "Experimental Images of inhomogeneous turbid media by frequency-domain diffusing-photon tomography", Optical Letters 20, 426-428 (1995).

[C17] van Houten, J., Bernaron, D., Spilman, S., and Stevenson, D., Imaging Brain Injury Using Time-resolved near-infrared light scanning, Pediatric Research 39, 470(1996).

[C18] Ishii, M., J.Leigh, and Schotland, J., in Optical Tomography, Photon Migration and Spectroscopy of Tissue and Model Media: Theory, Human Studies and Instrumentation (SPIE Optical Engineering Press, Bellingham, WA 1995), pp312.

[C19] Chang, J., Wang, Y., Aronson, R., Graber, H.L. and Barbour, R.L., SPIE Proceedings on Inverse Problems in Scattering and Imaging Vol. 1767, 384-391 (1992).

[C20] Chang, J.,R., Graber, and Barbour, R.L., in Imaging Reconstruction Dense Scattering Media Using Constrained CGD and a Matrix Scaling Technique (SPIE Optical Engineering Press, Bellingham, WA 1995), pp. 682-91.

[C21] Pogue, B.W., Patterson, M.S.,and Farrell, T.J. in Optical Tomography, Photon Migration and Spectroscopy of Tissue and Model Media:Theory, Human Studie and Instrumentation (SPIE Optical Engineering Press, Bellingham., WA 1995), pp328.

[C22] Schotland, J.C, Haselgrove, J. C., Leigh, J. S., "Photon hitting density", Applied Optics 1993, V23 N4:448-453.

[C23] Chance B, Kang K, He L, Weng J, and Sevick E,"Highly sensitive object location in tissue models with linear in-phase and anti-phase multi-element optical arrays in one and two dimensions," Proc. NAtl. Acad. Sci. , vol. 90, pp. 3423-3427, April 1993, Medical Science.

[C24] S. Zhou, S. Huang, C. Xie, H. Long, S. Kioka, B. Chance," Optical Imaging of Breast Tumor by Use of Dual Wavelngth Amplitude Cancellation System (phased array), Abstract, in Advances in Optical Imaging and Photon Migration, Sponsored by the Optical Society of America, March 8-11, 1998, Orlando Florida.

[C25] Q. Luo, S. Nioka and B. Chance, "Imaging on Brain Model by a Novel Optical Probe,"OSA TOPS on Advances in Optical Imaging and Photon Migration 1996, Vol 2. 155-159, R.R. Alfano and James G. Fujimoto (eds).

[C26] Chance B, Kang K, He L, Liu H and Zhou S,"Precision Location of Hidden Absorbers with Phased-Array Optical Systems, " Rev. Sci. Instru. 67 (12), 4324:4332, 1996.

[C27] Fishkin JB and Gratton E,"Propagation of photon-density waves in strongly scattering media containing an absorbing semi-infinite plane Bounded by a straight edge," J. Opt. Soc. Am. A 10, 127-140 (1993).

[C28] Fantini S, Franceschini MA and Gratton E,"Semi-infinite-geometry boundary problem for light migration in highly scattering media: a frequency-domain study in the diffusion approximation, J. Opt. Soc. Am. B. 11, 2128-2138, 1994.

[C30] Danen R.M., Wang Y., Li, X.D., Thayer W.S, and Yodh A.G., "Regional Imager for Low-Resolution Functional Imaging of the Brain with Diffusing Near-Infrared Light, "Photochemistry and Photobiology, 1998, 67(1):33-40

[C32]Zhu, Q., Chance, B, Sullivan, D, and Dambro, T. , "Combined Ultrasound and Near Infrared Diffused Light Imaging," IEEE Transactions on Ultrasonic, Ferroelectrics and Frequency Control, in press.

[C33] Hanley JA and McNeil BJ, "The Meaning and Use of the Area under a Receiver Operating Characteristic (ROC) Curve," Diagnostic Radiology, 143: 29:36, 1982.

[C34] J.B.Fishkin, O.Coquoz, E.R. Anderson, M.Brenner, and B.J. Tromberg,"Frequency-domain photon mogration measurements of normal and malignant tissue optical properties in human subject," Appl. Opt. 36,pp.10-20 (1997).

[C35] Q. Zhu et al., "A Novel Imaging Method Using a two-dimentional Ultrasound and Near Infrared Optical Array" will appear in Proc. of IEEE 1998 Ultrasonic Symposium.

Publications

Zhu, Q. Durduran, T and Yodh, A, "Novel Ultrasound and Optical Imaging Using a Two-dimentional Combined Array, Proc. IEEE Ultrasonic Symp.1998, in press.

Zhu, Q, "High Resolution Ultrasonic Imaging: Review of Acoustic Wavefront Distortion Compensation," Current Topics in Acoustical Research, A Review Series published by Research Trends, in press.

Zhu, Q., Chance, B, Sullivan, D, and Dambro, T. , "Combined Ultrasound and Near Infrared Diffused Light Imaging," IEEE Transactions on Ultrasonic, Ferroelectrics and Frequency Control, in press.

Zhu, Q. Chance, B, Sullivan, D, "Optically Guided Ultrasound Imaging System for High Specificity Breast Imaging," Proc. of SPIE (1997), SPIE Proc. of Optical Tomography and Spectroscopy of Tissue, pp. 48-58 (1997).

Zhu, Q. and Steinberg, B.D., "Modeling and Correction of Incoherent Wavefront Distortion" Special issue of I'nal. J. Sci. Tech. Imaging, Wiley, (03) 322:335, 1997.

Zhu, Q., and Steinberg, B.D., "Deaberration of Incoherent Wavefront Distortion: An Approach Toward Inverse Filtering," IEEE Transactions on Ultrasonic, Ferroelectrics and Frequency Control, (40), No.3, 575-589, May 1997.

Zhu, Q. and Chance, B, "A Novel Optically Guided Ultrasound Imaging System," Proc. IEEE Ultrasonic Symp. 1345-1348, 1996.

Zhu, Q. and Steinberg, B.D., "Toward Inverse Filtering Approach for Ultrasonic Wavefront Compensation," Proc. IEEE Ultrasonic Symp. 1357-1361 (1996).

Zhu, Q., Steinberg, B. D. and Arenson, R, "Correlation Distance Measurements of the Female Breast," J. Acoust. Soc. Am, (98) 694-705 (1995).

Zhu, Q. and Steinberg, B.D., "Correction of Multipath Interference by Spatial Location Diversity and Coherent CLEAN," Proc. IEEE Ultrasonic Symp, 1367-1370 (1995).

Hinkelman, L. M., Liu, D-L., **Zhu, Q.**, Steinberg, B. D. and Waag, R. C., "Measurement and Correction of Ultrasonic Pulse Distortion Produced by the Human Breast," J. Acoust. Soc. Am. (97) 1958-1969 (1995).

Presentations(1997-1999)

Zhu, Q., Chance, B, Sullivan, D, and Dambro, T. , "Combined Ultrasound and Near Infrared Diffused Light Imagin Ultrasonic Symposium, Oct. 1997, Toronto Canada

Zhu, Q, "Ultrasonic Wavefront Distortion Compensation in Pulse-Echo Using Toward Inverse Filtering Techniqu AIUM 42 Convention, March 1998, Boston .

Zhu, Q, Conant, E, and Chance, B., "Optical Imaging as an Adjunct to Ultrasound in Differentiating Benign from Malignant Lesions", SPIE Medical Optical Imaging, Feb 1999.

Zhu, Q., Durduran T., and Yodh, A., "Novel Ultrasound and Optical Imaging Using a Two-dimensional Combin Array". Ultrasonic Symposium, Oct. 1998, Saida Japan

Zhu, Q., Durduran T., and Yodh, A., "Novel Combined Ultrasound and Optical Imaging" SPIE Medical Optical Imaging, Feb. 1999.

STATEMENT OF WORK (Original)

Year One: Analyze the *in vitro* ultrasound transmission data previous acquired from 11 breast specimens. A detailed analysis of this large-aperture wavefront distortion data will result in a better understanding of the fundamental causes of wavefront distortion arising in ultrasound mammography. The statistics of wavefront amplitude distribution, useful 2-D aperture size, wavefront correlation distance will be determined. This information will guide the designs of the wavefront correction procedure and the 2-D concave cup array.

Year Two: Develop the proposed wavefront correction procedure and incorporate it into a commercial scanner. Perform phantom testing. Image quality, such as resolving power, sidelobe energy, etc., will be evaluated before and after application of correction procedure.

Year Three: Study the trade-offs among various design parameters of a 2-D concave array (see Section d3) through computer simulation. Optimize radiation pattern with respect to beamwidth, sidelobe level and total number of array element. Select designs for radiation pattern measurement.

Year Four: Develop a measurement procedure for radiation pattern testing. Measure radiation patterns of selected designs using the water tank apparatus and a breast phantom. Select the final design based on beamwidth, sidelobe level and total number of array elements.

REVISED STATEMENT OF WORK

Year One: No change.

Year Two: Developed a novel wavefront compensation algorithm called Toward Inverse Filtering (TIF). Experimentation with TIF using data obtained from in vitro breast samples. Comparisons of TIF with other compensation algorithms. In addition to TIF, another novel compensation approach which we called modified CLEAN algorithm (MCLEAN), although it had limitations in its application to breast imaging, was also exploited. MCLEAN has shown to improve image quality by canceling coherent multipath image artifacts. The strengths and limitations of MCLEAN were investigated.

Year Three: Designed, fabricated and constructed a planar two-dimensional ultrasound array. Preliminary electrical and acoustic testing of the array. Demonstrated potential utility of combining near infrared (NIR) optical method with ultrasound to improve breast cancer detection.

Year Four: Developing a small-scale ultrasound scanner consisting 20-channel front end electronics for acquiring data from a two-dimensional ultrasound array. Test the array radiation pattern in water tank. Apply ultrasonic wavefront compensation algorithms developed in year one and two to in vitro breast sample or phantom data that will be obtained with the two-dimensional array.

Develop a two-dimensional NIR array and NIR optical data acquisition system. Construct a combined 2-dimensional NIR and ultrasound array. Test the combined imaging technique in cancer detection using phantoms.